DEVELOPMENT OF WIDE-BANDGAP II-VI SEMICONDUCTOR LIGHT-EMITTING DEVICE TECHNOLOGY BASED ON THE GRADED INJECTOR DESIGN

Thesis by

Johanes F. N. Swenberg

In Partial Fulfillment of the Requirements

for the Degree of

Doctor of Philosophy

California Institute of Technology

Pasadena, California

1995

(Defended April 14, 1995)

to

my family

Acknowledgments

I will forever be grateful for the unique opportunity of being part of the Caltech community. More importantly, I am thankful for having been a member of the McGill group. I wish to express my gratitude for this unique opportunity. Tom McGill has created a rich and rewarding environment for graduate research, and personal and professional development. I have grown immeasurably these past years. His creative teaching, mentoring and friendship have prepared me for an exciting and uncertain future.

Any successful organization's greatest asset is its people. This has clearly been the rule with Tom McGill's group of individuals he has brought together. It has been a privilege and pleasure working and interacting with these talented people. Perhaps the most valuable asset in Tom's operation has been Marcia Hudson. Without her the group would soon lose its momentum. Marcia has been a trusted friend and accomplice.

My early interactions with former students gave me a good foundation for my subsequent research. Mike Jackson, Dave Chow, and Ed Croke along with other older students served as good examples to learn from. My earliest experimental research exposure with Yasantha Rajakarunanayake benefited me in the following years.

I owe a great deal to Mark Phillips for his guidance and instruction in the cleanroom and with the II-VI MBE machine. If he succeeded in transferring a small fraction of his skills, abilities and knowledge to me, I can call myself a great

experimentalist. Many thanks to Doug Collins for his patience trying to instruct me in the ways of III-V MBE. I owe him many beers. Working the past years with Mike Wang on the II-VI project has been very rewarding. I have enjoyed our times in the cleanroom, but I had preferred the good dim sum.

The group as a whole and myself have benefited tremendously from our interactions with senior researchers. I consider myself extremely lucky to have shared a conversation or heard their stories. Dr. J. McCaldin has been the creative mind behind the II-VI project. I am constantly amazed at his past and present accomplishments. Ogden Marsh has been a great source of ideas and reality checks. Andy Hunter has helped directly with early Hall experiments.

My interactions with the members of the group have contributed to my accomplishments and happiness these past years. Naturally, all the individuals who have participated in maintaining the computers and network have made this thesis and daily life possible. I thank you all for your valuable expertise. Dave Ting has been a great theorist and realist to share a conversation. He and the other theorists in the group have changed my earlier preconceptions about theorists. Ron Marquardt was a great roommate and labmate in spite of his magnet. He will long be remembered in the group. Yixin Liu has added a valued cultural and culinary experience to the group. I am impressed with his uncanny ability to answer all my questions. Harold Levy has been way cool. Totally incredible mind, dude. Chris Springfield has brought a complementary artistic creativity to the group each of us has been enriched by. I am glad I will one day be able to say, "Yes, I know the director of that film. I went to school with him." Shaun Kirby was a good officemate and fellow Republican to talk with. I'm sorry our times at Caltech did not overlap more. Of course Rob Miles and I have much in common and many debates for when we disagreed. It is always a pleasure to find a fellow conservative and patriot. I will miss his comradery. I have truly enjoyed the turbo-charged energy of Per-Olov Pettersson. I greatly admire and respect his creative ideas, curiosity, and shared value in the all-mighty-dollar. All total, my friendship with

the members of the group will far outlast what I learned at Caltech.

Having watched many newer students join the group, I think I understand some of Tom's enthusiasm with teaching fresh young minds. Alicia Alonzo, Xiao-Chang Cheng, Erik Daniels and Eric (Speakers) Piquette have been exciting to see grow and contribute so quickly. I wish them much luck.

Outside of school, the faithful companionship of both Babe and Toddy (my wife's and my dogs), has enriched our happy and comforting home. They have helped balance my life and maintain my sanity.

Without the support and encouragement of my friends and family I don't know where I would be today. My parents have and would sacrifice anything for my betterment. I love them dearly and thank them for their wisdom and strength. My big brother, Chuck, has been a valued mentor and best friend.

Finally, I thank my wife Linda Swenberg for her love, support, and patience. She has given greater meaning for my struggles and hard work. Bless you.

Abstract

This thesis describes the technical development of a novel semiconductor device design aimed at realizing short wavelength visible light emitters. The device structure, called the graded injector, achieves minority carrier injection in a heterojunction system with unfavorable type-II band alignment. Band edge engineering with an alloy graded intermediary layer effectively reduces the conduction band offset and allows for efficient minority carrier injection. The basic device structure consists of a n-CdSe/$Mg_xCd_{1-x}Se$/p-ZnTe heterojunction, where the $Mg_xCd_{1-x}Se$ region is graded.

The device design, materials growth, and characterization of II-VI green LEDs based on this structure are presented. Simulations demonstrate the operating principle of the graded injector. Early device development had been hindered by the lack of a p-type dopant for MBE ZnTe and the unavailability of high quality substrates. These restrictions have been overcome with the development of efficient nitrogen p-type doping of ZnTe and the growth capability of high quality heteroepitaxy on GaSb substrates. The materials characterization of the Mg-chalcogenides has enabled more accurate band edge engineering necessary for an operating device.

The advances in growth technology and materials characterization have been incorporated to grow and fabricate working graded injector LEDs. The operating characteristics of these devices unequivocally demonstrate the diode-like operation and efficient minority carrier injection. The electrical and optical performance of these devices will be presented and analyzed.

Contents

List of Figures

Glossary of Acronyms

LED	light-emitting diode
LD	laser diode
DH	double heterojunction
SH	single heterojunction
CW	continuous wave
MBE	molecular-beam epitaxy
MOCVD	(=OMVPE=MOVPE) metalorganic chemical vapor deposition
UHV	ultra-high vacuum
RGA	residual gas analyzer
RHEED	reflection high energy electron diffraction
CIE	Commission Internationale de L'Eclairage
FWHM	full width half maximum
CBE	conduction band edge
VBE	valence band edge
VBO	valence band offset
MIS	metal-insulator-semiconductor
PL	photoluminescence
EL	electroluminescence

RF	radio frequency
ECR	electron cyclotron resonance
TEM	transmission electron microscopy
AFM	atomic force microscopy
XPS	X-ray photoemission spectroscopy
QE	quantum efficiency

List of Publications

Work related to this thesis has been, or will be, published under the following titles:

Advances in the development of graded injector visible light emitters , J. F. Swenberg, M. W. Wang, R. J. Miles, M. C. Phillips, A. T. Hunter, J. O. McCaldin, and T. C. McGill, *J. Cryst. Growth* **138**, 692 (1994).

X-ray photoelectron spectroscopy measurement of valence-band offsets for Mg-based semiconductor compounds, M. W. Wang, J. F. Swenberg, M. C. Phillips, E. T. Yu, J. O. McCaldin, R. W. Grant, and T. C. McGill, *Appl. Phys. Lett.* **64**, 3455 (1994).

Measurement of the MgSe/$Cd_{0.54}Zn_{0.46}Se$ valence band offset by X-ray photoelectron spectroscopy, M. W. Wang, J. F. Swenberg, R. J. Miles, M. C. Phillips, E. T. Yu, J. O. McCaldin, R. W. Grant, and T. C. McGill, *J. Cryst. Growth* **138**, 508 (1994).

Investigation of crystal quality and surface morphology of ZnTe:N epilayers grown on ZnTe and GaSb substrates, R. J. Miles, J. F. Swenberg, M. W. Wang, M. C. Phillips, and T. C. McGill, *J. Cryst. Growth* **138**, 523 (1994).

n-CdSe/p-ZnTe based wide band gap light emitters: numerical simulation and design,

M. W. Wang, M. C. Phillips, J. F. Swenberg, E. T. Yu, J. O. McCaldin and T. C. McGill, *J. Appl. Phys.* **73**, 4660 (1993).

A new approach to wide band gap visible light emitters,

M. C. Phillips, J. F. Swenberg, M. W. Wang, J. O. McCaldin and T. C. McGill, *Physica B* **185**, 485 (1993).

Proposal and verification of a new visible light emitter based on wide band gap II-VI semiconductors,

M. C. Phillips, M. W. Wang, J. F. Swenberg, J. O. McCaldin and T. C. McGill, *Appl. Phys. Lett.* **61**, 1962 (1992).

Forming of Al-doped ZnTe epilayers grown by molecular beam epitaxy,

M. C. Phillips, J. F. Swenberg, Y. X. Liu, M. W. Wang, J. O. McCaldin and T. C. McGill, *J. Cryst. Growth* **117**, 1050 (1992).

Chapter 1

Introduction

This thesis describes major advances in the development of a novel device design proposed for wide band gap semiconductor visible light emitters. The standard approach to wide band gap semiconductors has traditionally focused on addressing the doping constraints which have plagued these materials. The long standing inability to dope the wide band gap semiconductors both n and p-type in the same material had frustrated the fabrication of diode structures. The device design presented in this thesis, called the graded junction electron injector or "graded injector" for short, offers an alternative approach to realizing diode behavior from heterostructure wide band gap materials. This device avoids the major doping obstacles associated with the wide band gap semiconductors. The operating principles of this device provides a means for achieving minority carrier injection in a heterojunction system with unfavorable band alignments.

The major contributions in this thesis have been the successful p-type doping of ZnTe by MBE, the high quality heteroepitaxy of ZnTe on III-V (GaSb) substrates, and the materials characterization of $Mg_xCd_{1-x}Se$. The results of this materials growth and characterization development have been successfully implemented to realize working LEDs based on the graded injector design. The operating characteristics of these devices have been dramatically improved over the first reported

working devices, and unequivocally demonstrate the diode operation of our heterostructure design. This first chapter offers motivation for interest in the wide band gap materials, and discusses the relevance of our device to shorter wavelength visible light emitters.

1.1 Motivation

The commercialization of visible light emitting devices (LEDs) began in the early 1960's following the work of Holonyak and Bevacqua [1]. Since then the optical performance of commercial visible LEDs has increased by over two orders of magnitude (Figure 1.1). This dramatic performance gain has been achieved through significant advancements in materials and growth technologies coupled with improved device engineering. The net effect is an over $1 billion per year market (1992 market) for visible LEDs with more than 20 billion diode chips produced each year [2]. The visible LED market is in fact the largest segment of the compound semiconductor device market comprising 37% of the overall market revenue in 1992 [3]. By contrast, during the same year the laser diode (LD) market commanded only an 11% share of the compound semiconductor market with worldwide production exceeding 49 millions units and revenues of roughly $287 million.

We expect the market and demand for visible LEDs to continue to grow. This will result largely from the development of higher performance devices which have enabled their introduction into new products and applications. High efficiency LEDs are in fact the devices of choice over incandescents for most applications due to their long lifetimes (approaching 10^6 hours), sharp linewidths for spectral purity, fast switching times, and reduced power consumption. As visible LED performance has improved, the range of applications has grown from small indicators used in low light level environments to larger displays and indicators used in outdoor sunlight environments.

The human eye's response to visible light depends strongly on the wavelength.

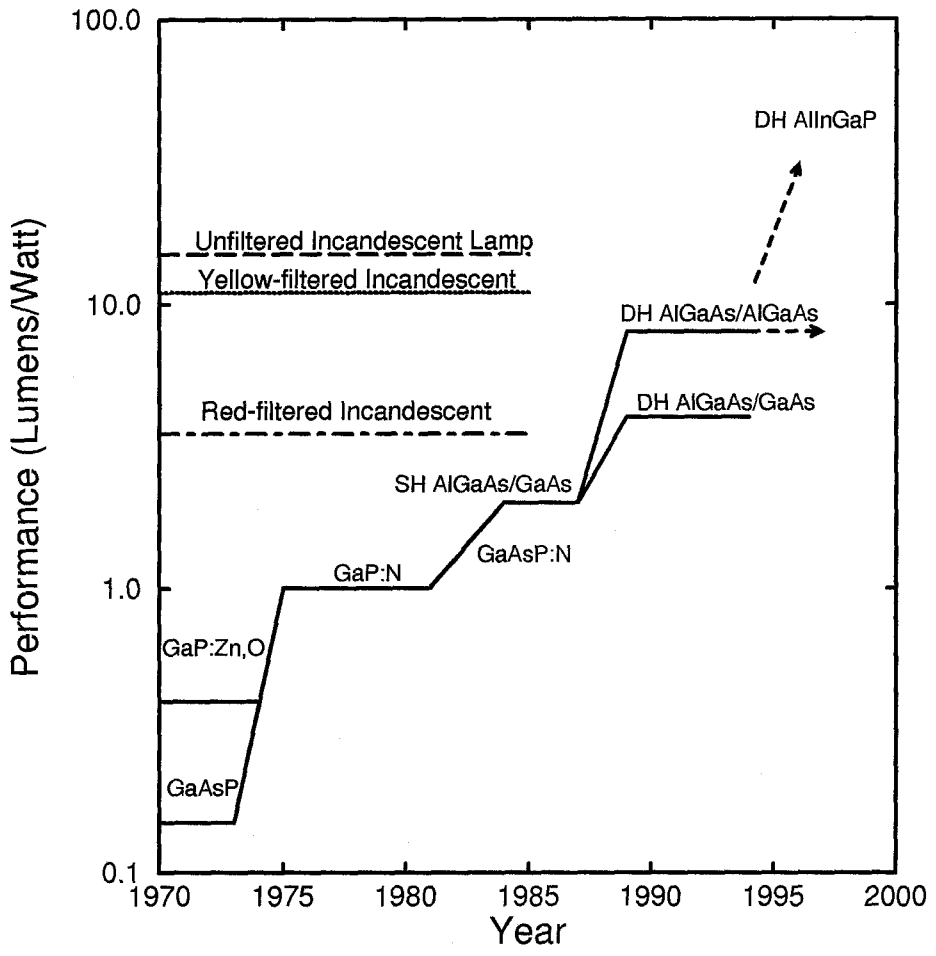

Figure 1.1: Evolution of commercial visible LED performance [2]. The luminous performance (lumens/watt) is calculated by multiplying the power efficiency (optical output power/electrical input power) by the human's eye response function defined by the Commission Internationale de L'Eclairage, or CIE. Thus, the performance is measured relative to the eyes sensitivity. Double-heterostructure (DH) devices outperform single-heterostructure (SH) devices. For the AlGaAs/GaAs structure, a GaAs absorbing substrate is present, while for the AlGaAs/AlGaAs structure the GaAs substrate is removed and a transparent AlGaAs "substrate" remains. DH red AlGaAs LEDs perform better than red-filtered incandescent lamps. AlInGaP promises to be brighter than AlGaAs in the yellow and possibly in the red as well.

It is most sensitive in the green region of the spectrum and less so into the red and blue. A plot of the relative eye sensitivity is found in figure 1.3. Due to this wavelength dependence, we need a measure other than optical power to quantify the visual response to a generic light source. We do this by using photometric units rather than their radiometric counterparts. Radiometric quantities deal solely with the energy content of optical radiation. An example is the radiant flux, more commonly refered to as optical power, measured in units of watts. On the otherhand, photometric units are defined to quantify the visual response produced by a light source. The photometric analog to the radiant flux (power) is the luminous flux, measured in lumens (lm). The luminous flux is essentially the integral of the spectral radiant flux over the visible wavelengths weighted by the eye response [4]. Therefore, the lumen quantifies a visible light source by incorporating the eye's sensitivity to the radiation. This enables quantitative comparisons between different light sources independent of spectral characteristics. Using photometric units, we refer to a device's luminous performance (lm/W), or simply performance, as the ratio of the light output in lumens to the electrical input power in watts.

Early red LEDs had luminous performances of 0.15 lm/W and were suitable for many indoor applications such as indicator lamps and numeric displays. Although, these devices were significantly outperformed by 3.5 lm/W red-filtered incandescent lamps. The double-heterostructure (DH) AlGaAs/AlGaAs red diodes developed in the late 1980's exceeded the performance of red-filtered incandescent lamps. This opened a large and growing market for outdoor indicator lamps such as automotive brake lights and message panels. The advancement of AlInGaP technology beginning in 1990 [5], with performance roughly ten times better than existing yellow LEDs and comparable to the highest performance red DH AlGaAs LEDs, extended the high performance of LEDs into the orange and yellow regions of the visible spectrum. Together these devices will find growing use in areas demanding high flux and/or low power consumption.

Much of the commercial success for visible LEDs has occurred in spite of the fact

that LEDs operating in the green and blue have not shared in the remarkable performance gains of the longer wavelength yellow-red LEDs. The present commercial green (GaP) and blue (SiC) LEDs are not suitable for more advanced applications. They presently are restricted to small and restrictive markets. Furthermore, these materials can not be advanced technologically to any great degree in terms of optical performance or making LDs due to their indirect band gap. The availability of high performance blue and green LEDs comparable to the commercial yellow and red would not only enable the use of green and blue LEDs for additional outdoor indicators but would open entirely new markets to LEDs. A high brightness green LED, for example, would offer a totally solid-state solution to traffic lighting. This would lead to faster, brighter, and spectrally sharper lights demanding less energy and maintenance. The combination of blue and green high brightness LEDs along with red would enable the creation of full-color large-area displays. Additionally, high-brightness LEDs can replace other light sources for non-display applications such as in copiers and printers. Therefore there is tremendous commercial and technological interest in developing more advanced short wavelength LEDs.

It should be noted that an equal if not greater interest exists in developing shorter wavelength laser diodes. This results from system's demanding shorter wavelength LDs, such as high capacity compact discs players and high performance color laser printers. Unit sales and revenue of shorter wavelength LDs may fall short of comparable wavelength LEDs, but the value added to systems would be significant and possibly greater than for short wavelength LEDs. Therefore, shorter wavelength LDs and LEDs are of equal interest commercially. In fact, the solutions to realizing both commercially viable LDs and LEDs will share similar technological developments. Both, for instance, will need to address similar types of materials, growth and device engineering issues.

1.2 Present commercial LEDs

Figure 1.2 illustrates the trends and differences in device performance (lumens/watt) of existing commercial LEDs as a function of their emission wavelength. Viewed another way, figure 1.3 plots the external quantum efficiencies for various commercial LEDs as a function of the peak emission wavelength. Both figures highlight the dramatically reduced performance of LEDs as the emission wavelength is reduced. This phenomena is due to the inherently poor radiative efficiency of indirect band gap semiconductors. Both GaP and SiC are indirect gap materials and AlInGaP approaches an indirect gap material as the band gap increases. The drop-off in performance of the AlInGaP with increasing band gap is expected as the direct-indirect gap transition is approached and carriers are lost to the higher energy indirect minima.

1.3 Development of short wavelength LEDs

The need for shorter wavelength LEDs and the inadequacies of the standard III-V semiconductors used in visible LEDs has led to an interest in alternative wide band gap materials. The most likely candidates have long been the wide band gap II-VI and the III-V nitride (GaN, AlN, InN) semiconductors. These materials with their wide band gap from the green through the blue and into the UV are most attractive for short wavelength light emitters. However, two areas have consistently plagued the development of light emitters based on the wide band gap materials. The difficultly in achieving low resistivity amphoteric doping (doping both p and n-type in the same material) required for electron and hole injection and the lack of suitable lattice matched substrates for homoepitaxial growth have hindered these material potentials from being realized.

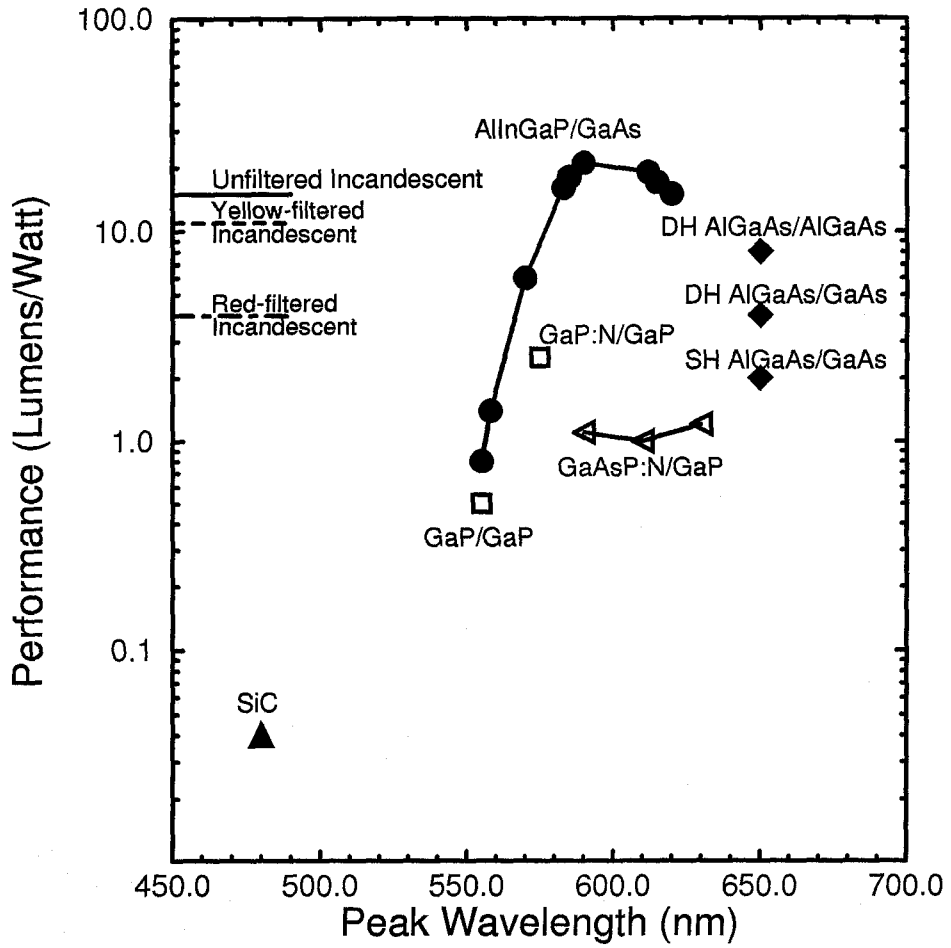

Figure 1.2: LED luminous performance as a function of emission wavelength [2]. High efficiency red and yellow LEDs based on the III-V semiconductors outperform filtered incandescent lamps. AlGaAs LEDs are only available in one color, but the AlInGaP quaternary can span the colors from green to red. Unfortunately, the AlInGaP system becomes less efficient as the emission wavelength becomes shorter. This results from a transition from direct to indirect band gap with increasing Al concentration. Indirect semiconductors, like GaP are inherently inefficient light emitters and can not achieve the performance demanded of high brightness LEDs.

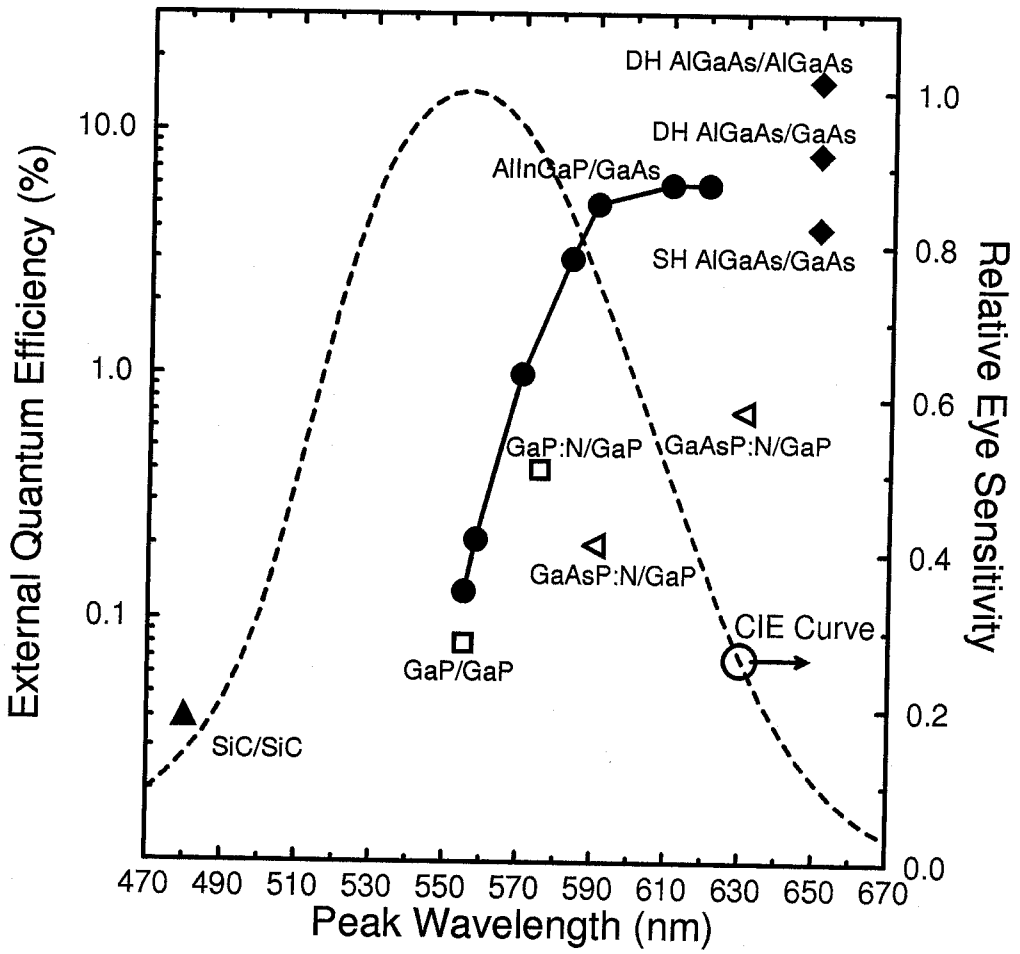

Figure 1.3: External quantum efficiencies (photons emitted from device/electrons passing through device) for various commercial LEDs as a function of peak emission wavelength. Also plotted with a dashed line is the CIE eye-response curve.

1.3.1 ZnSe based devices

For decades the most popular wide band gap material for short wavelength visible light emitters has been ZnSe, due to its large band gap in the blue, and close lattice match to GaAs substrates. The major obstacles have been the inability to grow p-type ZnSe. There had been many attempts to grow p-type ZnSe using various growth and doping techniques [6]. Most approaches have been unsuccessful due to compensation of the incorporated acceptor species, lack of solubility or the formation of deep levels. The dopant Lithium received attention following Nishizawa's *et al.* [7] reported growth of p-type ZnSe. They used the temperature difference solution growth method, a bulk crystal growth technique, under controlled vapor pressure to grow p-type ZnSe crystals. They also reported working p-n diodes with blue light emission. Soon afterwards, in 1988, Cheng *et al.* [8] reported the first p-type conversion of ZnSe grown by MBE using Li. Although they initially only achieved free hole carrier concentrations of $3.6\times10^{13}\text{cm}^{-3}$, net acceptor concentrations as high as $8.0\times10^{16}\text{cm}^{-3}$ and resistivities as low as 2.9 Ω-cm were later reported [9], and p-n junction blue LEDs were successfully grown using Li as the p dopant [9, 10, 11]. Unfortunately, two major obstacles limited the usefulness of Li as a p-type dopant in ZnSe. First, the net acceptor concentration saturates at $8.0\times10^{16}\text{cm}^{-3}$, a level too low for suitable ohmic contacting, and with higher Li incorporation compensation processes occur resulting in highly resistive ZnSe [9]. Second, Li is an unstable dopant, known to diffuse interstitially in ZnSe quite rapidly [9, 12].

Nitrogen had also received considerable attention as a likely candidate p-type dopant. Stutius [13] suggested that nitrogen is the most promising element for a p-type dopant, taking into account problems with the other likely candidates such as Li, Na, P, and As. Dean *et al.* [14] identified nitrogen impurities in ZnSe resulted in the incorporation as a shallow acceptor state with an activation energy of $\sim$ 110 meV. Park *et al.* [15] demonstrated the incorporation of nitrogen accep-

tors in ZnSe during MBE and confirmed an activation energy of $\sim$ 110 meV. In this work they used neutral N_2 and NH_3 and managed to incorporate only small concentrations of nitrogen impurities due to the low sticking coefficient and solubility of the nitrogen molecular species. Mitsuyu *et al.* [16] apparently succeeded in enhancing incorporation of nitrogen impurities in MBE ZnSe by employing a low-energy ionized beam of NH_3. Unfortunately, in both these experiments p-type conduction was not observed. Although N was believed to be a suitable p-type dopant, an appropriate method of incorporating sufficient concentrations of the impurity during MBE remained to be discovered.

A tremendous breakthrough occurred when Park *et al.* [17] and Ohkawa *et al.* [18] working independently discovered that by employing an RF plasma discharge doping incorporation of N in ZnSe was enhanced. N incorporation up to $1.0\times10^{19}\text{cm}^{-3}$ [18] and net acceptor concentrations as large as $3.4\times10^{17}\text{cm}^{-3}$ [17] were achieved for the first time. p-n homojunction LEDs exhibiting blue luminescence based on p-ZnSe:N/n-ZnSe:Cl were also reported at this time by Park [17]. The dramatic doping success was soon followed by the announcement from 3M [19] of the first demonstrated operation of a blue-green (490nm) laser diode operating under pulsed current injection at 77K.

In spite of the successes of N doping of ZnSe many obstacles associated with this material system remain unsolved. The first noted problem was the saturation in the maximum net acceptor concentration (N_A - N_D), using N, at roughly $1\times10^{18}\text{cm}^{-3}$ [20]. These levels of doping are sufficient for low resistivity epilayers for LEDs and LDs but are by themselves insufficient for ohmic contacts. In fact this doping saturation problem is exacerbated as the band gap of ZnSe is increased with the addition of Mg and S forming $Mg_xZn_{1-x}S_ySe_{1-y}$. This alloy allows for tuning of the band gap of the layers for a given lattice constant. Okuyama *et al.* [21, 22] demonstrated the use of the $Mg_xZn_{1-x}S_ySe_{1-y}$ alloy for electrical confinement and optical cladding in separate confinement heterostructure blue laser diodes [23, 24, 25]. Unfortunately, the p-type doping of $Mg_xZn_{1-x}S_ySe_{1-y}$ is com-

plicated by a dramatic decrease in the maximum net acceptor concentration and increase in the energy of the nitrogen acceptor level with increasing band gap [26]. Therefore laser threshold and operating voltages increase as the operating wavelengths decrease [27, 28].

The doping difficulties have been proposed to be fundamentally related to "self-compensation" effects (through dopant lattice relaxation [29] or the generation of donor-like centers during growth [30, 31, 32]) or due to acceptor solubility limitations [33]. Nevertheless, considerable progress has been made in overcoming these doping limitations by engineering novel ohmic contacting schemes. A pseudograded band gap Zn(Se,Te) [34] epilayer, resonant tunneling multiquantum well ZnTe/ZnSe [35] epilayer, and HgSe [36] contacting layer all succeeded in reducing contacting resistances to levels acceptable for LEDs and LDs. Subsequently, low voltage operation (< 4 Volts) of ZnSe based blue and green LEDs [37], and low voltage ($V_{th} \sim 4.4$ V) room temperature operation of blue-green laser diodes [27, 28] were demonstrated.

The continued advancement of ZnSe based light emitters has progressed to the point where LED structures operating in the blue and green have performances (1.6 lm/W 489nm, 17 lm/W 512nm) [40] as good as commercial red. The green LEDs have maximum external quantum efficiencies of 5.3%. Despite these accomplishments, the ZnSe based devices face a major challenge relating to the issue of stability and operating lifetime. The blue and green LEDs, while performing orders of magnitude better than their commercial conterpart, are severly limited in device lifetime. Improvements in bulk growth technology of ZnSe [38, 39] has resulted in high quality ZnSe with x-ray full width at half-maximum (FWHM) of 11-16 arcsec, indicating crystal quality comparable to that of GaAs substrates. Homoepitaxial devices grown on on these substrates have the best lifetimes, although even operating under optimal conditions ($J = 15$ A/cm^2) these LEDs' light output decay exponentially with a time constant of only 675 hours [40]. As for the laser diode, the longest published continuous wave operation at room temperature is

one hour [41].

Guha *et al.* [42] studied the degradation of ZnSe light emitting devices, and showed that the degradation was related to the formation of new crystal defects from the vicinity of pre-existing defects such as stacking faults and these defects propagated throughtout the active region and enhanced nonradiative recombination. They further found that these stacking faults originated at the epilayer/substrate(GaAs) interface during the initial stages of the growth [43]. Additional studies have shown that the incorporation of nitrogen affects the structural properties of ZnSe, with the generation of point defects accompanying N doping [44], and an increase in the formation of stacking faults [45]. The success or failure of the ZnSe devices will largerly depend on overcoming these degradation problems. While this may be possible to achieve through improved growth technology, it could prove to be intractable if the material stability is fundamentally associated with the nitrogen doping.

1.3.2 Nitride based devices

The III-V nitrides (InN, GaN, AlN) have also been viewed as promising materials for short wavelength light emitters [46], because the wurtzite polytypes of InN, GaN, and AlN form a continuous alloy sytem whose direct band gaps range from 1.9 eV for InN, to 3.4 eV for GaN, to 6.2 eV for AlN. Additionally, these materials possess physical hardness, large band offsets, high thermal conductivity, and high melting temperatures [47]. The major obstacles, similar to those of ZnSe, have been the lack of a suitable substrate material that is lattice matched and thermally compatible with the nitrides and the difficulty in achieving p-type conductivity.

Due to the lack of a suitable substrate, it has been difficult to grow epitaxial GaN films of high quality. For lack of an ideal substrate, most nitride material has been grown on sapphire substrates despite a huge lattice mismatch ($\sim$13.8%) and large difference in thermal expansion coefficients. This choice of substrate is

attributed to its availability, hexagonal structure, ease in handling, and thermal stability at elevated growth temperatures. Consequently, much work has been devoted to the understanding and development of epitaxy of nitrides on lattice mismatched substrates [48]. A major improvement in the structural quality of GaN epilayers was accomplished by using an AlN buffer layer between the grown GaN film and sapphire substrate in both MBE [49] and MOVPE [50] growth. Nakamura *et al.*, subsequently discovered that a thin buffer layer of GaN grown at lower growth temperatures could also produce similar results.

The longstanding problem of p-type doping of GaN was frustrated by compensation processes leaving only highly resistive material. Nevertheless, GaN LEDs had been reported over 20 years ago [51], but these devices were high field, low efficiency metal-insulator-semiconductor (MIS) structures. Recently however, Amano *et al.* succeeded for the first time in producing p-type GaN [52] and AlGaN [53]. As grown Mg-doped GaN layers had a hole concentration $p = 2\times10^{15}\text{cm}^{-3}$, and resistivity $\rho = 320\ \Omega$-cm. By using low energy electron beam irradiation (LEEBI) the electrical properties of the GaN were observed to change dramatically to $p = 3\times10^{18}\text{cm}^{-3}$, and resistivity $\rho = 0.2\ \Omega$-cm. Using this technique, Amano *et al.* developed the first conventional p-n junction GaN LED [52].

It was also discovered that compensated Mg-doped GaN could be converted equally well to p-type material by thermal annealing under an N_2 ambient [54]. This technique was an improvement over electron irradiation since it could convert the entire layer rather than only the irradiated regions. The compensation mechanism was identified as resulting from an Mg-H neutral complex formed during growth [55]. Soon afterwards, Moustakas *et al.* [56] reported the successful p-type doping of GaN grown by MBE using a solid source Mg cell as the dopant. They were able to achieved p-type material without post-growth processing due to the absence of H in the UHV environment of MBE.

With improvements in epitaxial material and amphoteric doping capabilities, it was not long before higher performance nitride LEDs were fabricated. Since

GaN has a band gap in the UV, the ternary alloy InGaN was the likely candidate for realizing visible light emitters since its band gap varies from 1.9 to 3.4 eV depending on the In concentration. The growth of high quality InGaN films obtained by Yoshimoto *et al.* [57], and the growth of Si-doped n-InGaN [58] lead to longer wavelength p-GaN/n-InGaN/n-GaN LEDs. A dramatic improvement in optical performance was realized with the successful Zn doping of InGaN in a InGaN/AlGaN DH blue LED [59]. Zn doping had been used in GaN [60, 61, 62] for strong below band gap emission. Incoporation of Zn in InGaN resulted in recomination emission 0.5 eV lower than the band edge emission of InGaN. This enabled the devices to operate in the blue. Quantum efficiencies as high as 2.7% were reported for these blue (450nm) LEDs, and they have been announced as a commercial product. Recently, external quantum efficiencies as high as 5.4% for blue (450nm) and 2.4% for blue-green (500nm) were reported by researchers from Nichia [63] using the InGaN/AlGaN DH structure. The optical performance of these LEDs and lifetimes of ten of thousands of hours make these devices commercially viable. In addition to the success of the nitrides in realizing commercial quality LEDs, recent reports of optically pumped near ultraviolet lasing from single-crystal GaN [64] has given encouragement for the propects of nitride based diode lasers in the near future.

Despite the remarkable results achieved with the nitrides in the past few years, there are still many issues which need to be addressed for commercial success. The present LED's optical characteristics suffer from very broad linewidths in the emission spectra, FWHM $\sim$ 70nm, due to the deep Zn recombination center. This broad emission seriously degrades the spectral purity. Ideally band to band recombination would be prefered over the deep Zn center (especially for lasing). This will require alloys with higher In concentrations. Generally, improved substrate material, ideally GaN, must be pursued to further improved material quality and enable the fabrication of laser diodes. Additionally, doping (primarily p-type), and processing and ohmic contacting technologies must also be improved for laser

development.

1.3.3 The graded injector

An alternative approach to realizing wide band gap light emitters based on the "graded injector" is discussed in this thesis. This novel device concept offers a unique approach to achieving minority carrier injection in a p-n heterojunction with unfavorable band offsets. Additionally this device avoids problems with amphoteric doping constraints and ohmic contacting by using materials which are capable of being readily doped either p-type or n-type. In spite of the above mentioned successes with ZnSe and GaN, the graded injector still remains of extreme technical interest due to its unique operation and potential application in the area of wide band gap semiconductors.

1.4 Outline

The remainder of the thesis is arranged as follows: Chapter 2 introduces the concept and basic design of the graded injector. The relevant issues necessary for a heterojunction diode are presented and incorporated in the device structure. Device simulations demonstrate the operating principle behind the graded junction.

Chapter 3 discusses the issues and details of the growth technology, molecular beam epitaxy (MBE), used to fabricate the graded injector LED. The choice and availability of appropriate substrates are presented. The p-type doping of ZnTe and the epitaxial growth of high quality ZnTe on GaSb substrates are presented.

Chapter 4 reports on the major advances in the development of the graded injector. Materials characterization and device engineering necessary for device development are present. Characterization of the device's material quality, electrical behavior and optical performance are discussed.

Bibliography

[1] N. Holonyak and S.F. Bevacqua, *Appl. Phys. Lett.* **1**, 82 (1962).

[2] M.G. Craford, *IEEE Circuits and Devices* **8, 24, (1992).**

[3] From data of M.G. Craford adapted from Strategies Unlimited report on Compound Semiconductor Device Market 1992. Net revenues totaled $2.8 billion.

[4] The lumen is defined as the luminous flux of monochromatic radiation at 555 nm whose radiant flux is equal to 1/683 W. For a discussion of photometric quantities and units see R.W. Boyd, *Radiometry and the Detection of Optical Radiation*, (John Wiley, New York, 1983), Chapter 6.

[5] C.P. Kuo, R.M. Fletcher, T.D. Osentowski, M.C. Lardizabal, M.G. Craford and V.M. Robbins, *Appl. Phys. Lett.* **57**, 2937 (1990).

[6] For a review of this work see R.N. Bhargava, *J. Cryst. Growth* **59**, 15 (1982).

[7] J. Nishizawa, K. Itoh, Y. Okuno and F. Sakurai, *J. Appl. Phys.* **57**, 2210 (1985).

[8] H. Cheng, J.M. DePuydt, J.E. Potts and T.L. Smith, *Appl. Phys. Lett.* **52**, 147 (1988).

[9] M.A. Haase, H. Cheng, J.M. DePuydt and J.E. Potts, *J. Appl. Phys.* **67**, 448 (1990).

[10] T. Yasuda, I. Mitsuishi and H. Kukimoto, *Appl. Phys. Lett.* **52**, 57 (1988).

[11] J. Ren, B. Sneed, K.A. Bowers, D.L. Dreifus, J.W. Cook, J.F. Schetzina and R.M. Kolbas, *Appl. Phys. Lett.* **57**, 1901 (1990).

[12] G.F. Neumark and S.P. Herko, *J. Cryst. Growth* **59**, 189 (1982).

[13] W. Stutius, *J. Cryst. Growth* **59**, 1 (1982).

[14] P.J. Dean, W. Stutius, G.F. Neumark, B.J. Fitzpatrick and R.N. Bhargava, *Phys. Rev. B* **27**, 2419 (1983).

[15] R.M. Park, H.A. Mar and N.M. Salansky, *J. Appl. Phys.* **58**, 1047 (1985).

[16] T. Mitsuyu, K. Ohkawa and O. Yamazaki, *Appl. Phys. Lett.* **49**, 1348 (1986).

[17] R.M. Park, M.B. Troffer, C.M. Rouleau, J.M. Depuyd and M.A. Haase, *Appl. Phys. Lett.* **57**, 2127 (1990).

[18] K. Ohkawa, T. Karasawa and T. Mitsuyu, *J. Cryst. Growth* **111**, 797 (1991).

[19] M.A. Haase, J. Qiu, J.M. Depuydt and H. Cheng, *Appl. Phys. Lett.* **59**, 1272 (1991).

[20] J.Qui, J.M. DePuydt, H. CHeng and M.A. Haase, *Appl. Phys. Lett.* **59**, 2993 (1991).

[21] H. Okuyama, K. Nakano, T. Miyajima and K. Akimoto, *Jpn. J. Appl. Phys.* **30**, L1620 (1991).

[22] H. Okuyama, K. Nakano, T. Miyajima and K. Akimoto, *J. Cryst. Growth* **117**, 139 (1992).

[23] K. Akimoto, H. Okuyama, T. Miyajima, T. Morinaga, F. Hiei and M. Ozawa, *Tech. Dig.* **2**, 306 (1993).

[24] J. Gaines, R. Drenton, K. Haberern, T. Marshall, P. Mensz and J. Petruzzello, *Appl. Phys. Lett.* **62**, 2462 (1993).

[25] J. Petruzzello, J. Gaines and P. van der Sluis, *Appl. Phys. Lett.* **75**, 63 (1994).

[26] H. Okuyama, Y. Kishita, T. Miyajima, A. Ishibashi and K. Akimoto, *Appl. Phys. Lett.* **64**, 904 (1994).

[27] A. Salokatve, H. Jeon, J. Ding, M. Hovinen, A.V. Nurmikko, D.C. Grillo, J. Han, L. He, Y. Fan, M.D. Ringle, R.L. Gunshor, G.C. Hua and N. Otsuka, *Electronics Letters* **29**, 2192 (1993).

[28] N. Nakayama, S. Itoh, H. Okuyama, M. Ozawa, T. Ohata, K. Nakano, M. Ikeda, A. Ishibashi and Y. Mori, *Electronics Letters* **29**, 2194 (1993).

[29] D.J. Chadi and K.J. Chang, *Appl. Phys. Lett.* **55**, 575 (1989).

[30] A. Ohki, Y. Kawaguchi, K. Ando and A. Katsui, *Appl. Phys. Lett.* **59**, 671 (1991).

[31] B. Hu, G. Karczewski, H. Luo, N. Samarth and J.K. Furdyna, *Appl. Phys. Lett.* **63**, 358 (1993).

[32] K.A. Prior, B. Murdin, C.R. Pidgeon, S.Y. Wang, I. Hauksson, J.T. Mullins, G. Horsburgh and B.C. Cavenett, *J. Cryst. Growth* **138**, 94 (1994).

[33] Y. Fan, J. Han, L. He, R.L. Gunshor, M.S. Brandt, J. Walker, N.M. Johnson and A.V. Nurmikko, *Appl. Phys. Lett.* **65**, 1001 (1994).

[34] Y. Fan, J. Han, L. He, J. Saraie, R.L. Gunshor, M. Hagerott, H. Jeon, A.V. Nurmikko, G.C. Hua and N. Otsuka, *Appl. Phys. Lett.* **61**, 3160 (1992).

[35] F. Hiei, M. Ikeda, M. Ozawa, T. Miyajima, A. Ishibashi and K. Akimoto, *Electronics Letters* **29**, 878 (1993).

[36] Y. Lansari, J. Ren, B. Sneed, K.A. Bowers, J.W. Cook and J.F. Schetzina, *Appl. Phys. Lett.* **61**, 2554 (1992).

[37] J. Ren, Y. Lansari, Z. Yu, J.W. Cook and J.F. Schetzina, *J. Elec. Mater.* **22**, 973 (1993).

[38] G. Cantwell, W.C. Harsch, H.C. Cotal, B.G. Markey, S.W.S. McKeever and J.E. Thomas, *J. Appl. Phys.* **71**, 2931 (1992).

[39] H. Cotal, B.G. Markey, S.W.S. McKeever, G. Cantwell and H.C. Harsch, *Physica B* **185**, 103 (1993).

[40] D.B. Eason, Z. Yu, W.C. Hughes, W.H. Roland, C. Boney, J.W. Cook, J.F. Schetzina, *Appl. Phys. Lett.* **66**, 115 (1995).

[41] S. Itoh and A. Ishibashi, *Proc. SPIE Conference on II-VI Blue/Green Laser Diodes*, R.L. Gunshor and A.V. Nurmikko, eds., SPIE (1994).

[42] S. Guha, J.M. DePuydt, M.A. Haase, J. Qiu and H. Cheng, *Appl. Phys. Lett.* **63**, 3107 (1993).

[43] S. Guha, J.M. DePuydt, J. Qiu, G.E. Hofler, M.A. Haase, B.J. Wu and H. Cheng, *Appl. Phys. Lett.* **63**, 3024 (1993).

[44] J. Petruzzello, J. Gaines, P. van der Sluis, D. Olego and C. Ponzoni, *Appl. Phys. Lett.* **62**, 1496 (1993).

[45] L.H. Kuo, L. Salamanca-Riba, J.M. DePuydt, H. Cheng and J. Qiu, *Appl. Phys. Lett.* **63**, 3197 (1993).

[46] For a review of the III-V nitrides see, S. Strite, M.E. Lin and H. Morkoç, *Thin Solid Films* **231**, 197 (1993)

[47] S. Strite and H. Morkoç, *J. Vac. Sci. Technol. B* **10**, 1237 (1992).

[48] For a review of substrates and nitride epitaxy see Ref. [47]

[49] S. Yoshida, S. Misawa and S. Gonda, *Appl. Phys. Lett.* **42**, 427 (1983).

[50] H. Amano, N. Sawaki, I. Akasaki and Y. Toyoda, *Appl. Phys. Lett.* **48**, 353 (1986).

[51] J.I. Pankove, E.A. Miller and J.E. Berkeyheiser, *RCA Rev.* **32**, 383 (1971).

[52] H. Amano, M. Kito, K. Hiramatsu and I. Akasaki, *Jpn. J. Appl. Phys.* **28**, L2112 (1989).

[53] H. Amano, M. Kito, K. Hiramatsu and I. Akasaki, *Inst. Phys. Conf. Ser.* **106**, 725 (1990).

[54] S. Nakamura, T. Mukai, M. Senoh and N. Iwasa, *Jpn. J. Appl. Phys.* **31**, L139 (1992).

[55] S. Nakamura, N. Iwasa, M. Senoh and T. Mukai, *Jpn. J. Appl. Phys.* **31**, 191 (1992).

[56] T.D. Moustakas and R.J. Molnar, *Materials Research Society Symp., Boston, MA*, 1992.

[57] N. Yoshimoto, T. Matsuoka, T. Sasaki and A. Katsui, *Appl. Phys. Lett.* **59**, 2251 (1991).

[58] S. Nakamura, T. Mukai and M. Senoh, *Jpn. J. Appl. Phys.* **31**, L16 (1992).

[59] S. Nakamura, T. Mukai and M. Senoh, *Appl. Phys. Lett.* **64**, 1687 (1994).

[60] J.L. Pankove and J.A. Hutchby, *Appl. Phys. Lett.* **24**, 281 (1974).

[61] H. Monemar, O. Lagerstadt and H.P. Gislason, *J. Appl. Phys.* **51**, 625 (1980).

[62] P. Bergman, G. Ying, B. Monemar and P.O. Holz, *J. Appl. Phys.* **61**, 4589 (1987).

[63] S. Nakamura, *IEEE IEDM, 567 (1994).*

[64] X.H. Yang, T.J. Schmidt, W. Shan, J.J. Song and B. Goldenberg, *Appl. Phys. Lett.* **66**, 1 (1995).

Chapter 2

The Graded Injector Light Emitter

2.1 Introduction

An LED's basic structure is a p-n junction diode. Figure 2.1 illustrates the band diagram for a simple p-n homojunction. Under a forward bias close to the band gap of the device material, minority carriers are injected into the recombination region of the device where they can recombine and emit light [1]. Commercial devices have been based on simple p-n homojunctions, where the p and n regions are the same binary or alloy material. More sophisticated structures, such as single- and double-heterostructures improve the recombination and extraction efficiencies but they are still based on the homojunction design [2].

This standard approach to LEDs has been sufficiently successful for narrow band gap materials, but has seen less success in the development of high efficiency green and blue LEDs. The fundamental problem in the development of wide band gap light emitters based on the II-VI semiconductors has been the inability of obtaining both n- and p-type doping in the same material. To some degree this restriction has been mitigated with the p-type doping of ZnSe by MBE [3, 4], but

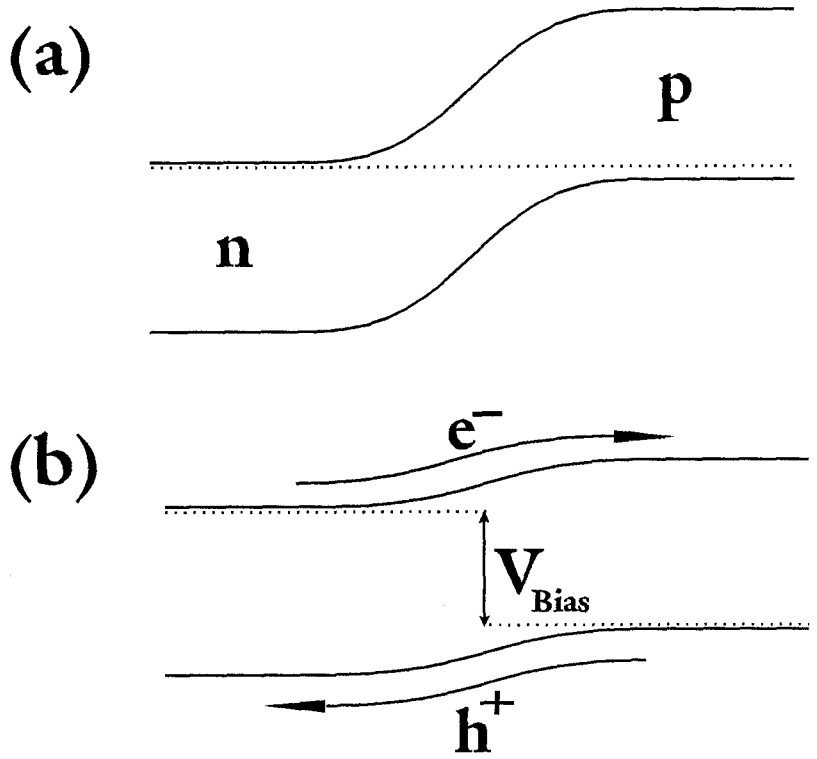

Figure 2.1: Schematic band diagrams for p-n homojunction at (a) zero bias and (b) under a forward bias V_{Bias}. The dashed line indicates the Fermi level in the unbiased diagram and the quasi-Fermi levels in the biased diagram. Under a forward bias, electrons are injected into the p-type material and holes are injected into the n-type material. The injected carriers then recombine with the majority charge carriers and emit light.

there remain several challenges ahead in the development of ZnSe based LEDs and laser diodes as previously discussed in chapter 1. An obvious yet non-trivial solution to avoid the doping problem is to use two different materials, one easily doped n-type and the other easily doped p-type, and form a heterojunction.

In this chapter, we examine a novel device concept based on a unique p-n heterojunction structure. This LED design is based on the only closely lattice matched II-VI binary compounds, namely n-CdSe and p-ZnTe. By taking advan-

tage of the natural doping types of these materials we avoid contacting and doping problems. An abrupt n-CdSe/p-ZnTe junction is found to be incapable of carrier injection. Using a properly graded alloy of $Mg_xCd_{1-x}Se$ placed between the CdSe and ZnTe junction we create a heterostructure capable of efficient minority carrier injection into the wider band gap ZnTe. Computer simulations illustrate the operating priciple of this graded injector LED.

2.2 Heterojunction approach

The basic paradigm to form a p-n heterojunction diode is to join a p-type material to a different n-type material. Forming a structure with these materials would by definition contain a p-n junction. In addition to using suitably dopable materials, there are strict constraints on lattice matching and band offsets necessary for a realistic device. In order to maintain material quality, lattice matched materials must be used, although small amounts of strain can be accomodated. As will be demonstrated below, whether a heterojunction device will be able to inject carriers will depend completely on the band offsets for that particular heterojunction structure.

To design a heterostructure device we need information on materials' band gaps, band offsets, dopabilities and lattice parameters. McCaldin [5] introduced a graphical technique to simultaneously present these parameters in a single diagram. By displaying all the relevant materials properties, these so called McCaldin diagrams allow one to easily choose suitable materials for a heterostructure device. Figure 2.2 shows a McCaldin diagram for some of the common II-VI binary compounds and other popular semiconductors. The band edge positions are plotted relative to the valence band of GaAs and are from the theoretical prediction of Harrison's linear combination of atomic orbitals (LCAO) theory [6]. The figure plots as a function of lattice constant the band edges of a semiconductor. The symbol for a material's band edge is filled/empty if the semiconductor can/cannot

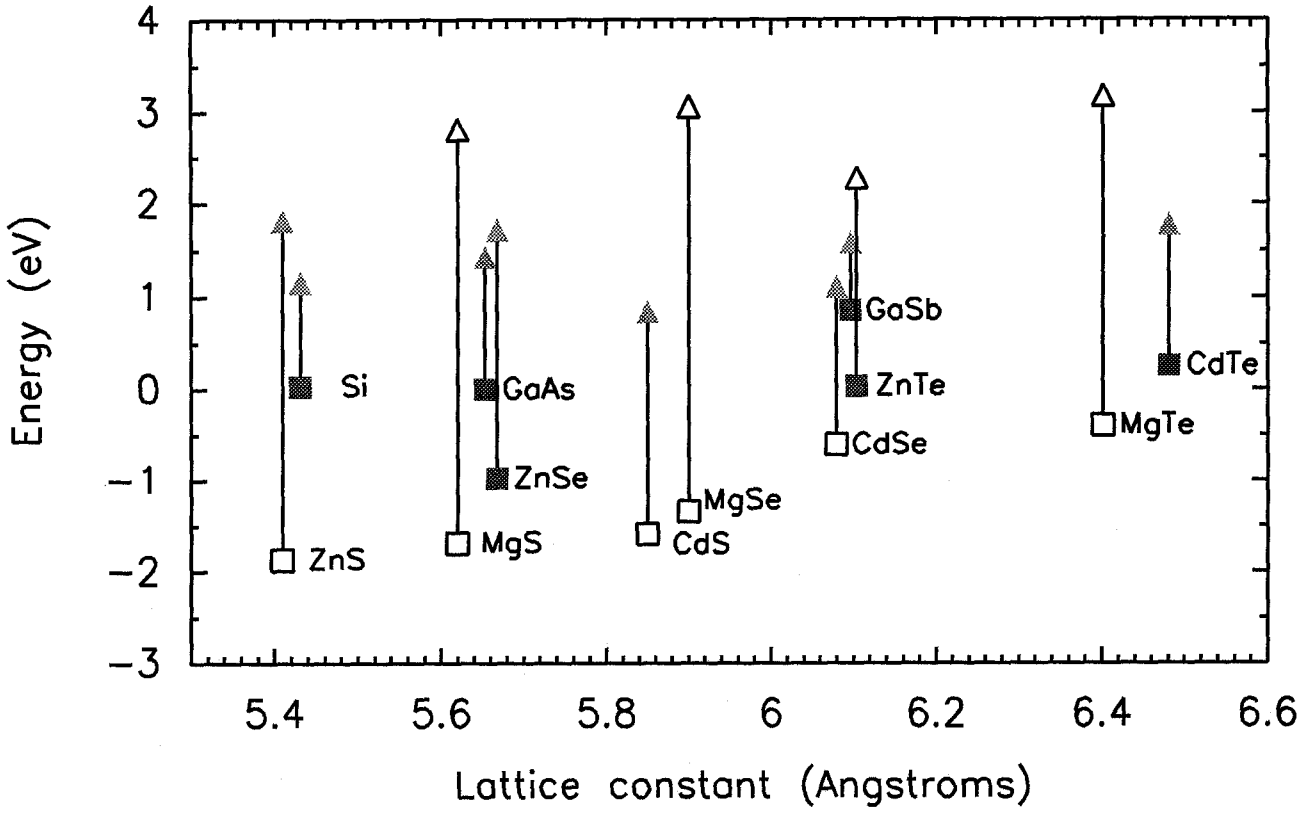

Figure 2.2: McCaldin diagram for various semiconductors. As a function of lattice parameter, the band edges of a semiconductor are plotted relative to the valence band of GaAs. This plot is from the valence band edge offsets calculated by Harrision [6]. The conduction band is indicated by a triangle and the valence band is indicated by a square. The band gap is given by the vetical line connecting the triangle and square. If the triangle/square is filled it indicates that the material can be conventionally doped n-type/p-type. If the shape is empty it means the material cannot be doped that type. Band offsets can be read from the diagram by the energy difference between band edges.

be doped that conductivity type. Yu *et al.* [7] provide a comprehensive review on the subject of band offsets and the salient issues associated with the theoretical and experimental results. We rely on the obvious trends displayed by the diagrams and make use of accepted experimental results for a given band offset to construct a heterojunction.

The use of heterojunctions to avoid the doping trends in the II-VI is an old idea. The most intensively investigated heterostructure among the II-VI semiconductors has been n-ZnSe/p-ZnTe [8, 9, 10]. Unfortunately, as can be seen in the Mccaldin diagram the extremely large 7% lattice mismatch between these materials proves to be disastrous for LED operation. McCaldin and McGill [11] recently proposed the n-AlSb/p-ZnTe junction as an electron injector into ZnTe based on the theoretical band alignment of Harrison [6]. Yu *et al.* [12] experimentally measured the band offset of AlSb/ZnTe and found the theroretical values to incorrectly predict the sign of the conduction band offset. Instead of the conduction band of AlSb lying above ZnTe, it was measured to be 0.21 eV below. Attempts to fabricate n-AlSb/p-ZnTe diodes by Han *et al.* [13] demonstrated the inability of obtaining electron injection for this heterojunction.

We can notice various trends in doping when a larger collection of materials are plotted using different theoretical calculations and experimental data. It seems to hold, as suggested [14, 15], that the positions of the valence and conduction band edges with respect to some absolute energy scale are an important factor in doping. Generally we see, the lower the position of the valence band edge, the more difficult the material is to be doped p-type and, similarly, the higher the conduction band edge, the more difficult it is to be dope n-type [5]. This appears to hold true for the selenides, sulfides and ZnTe. We should note that ZnTe is the only wide band gap II-VI compound which is conventionally doped p-type. Unfortunately, the doping trends evident in the McCaldin diagrams counter the need for either an n-type material with a high conduction band or a p-type material with a low valence band. This is the same impediment with wide band gap II-VI homojunctions,

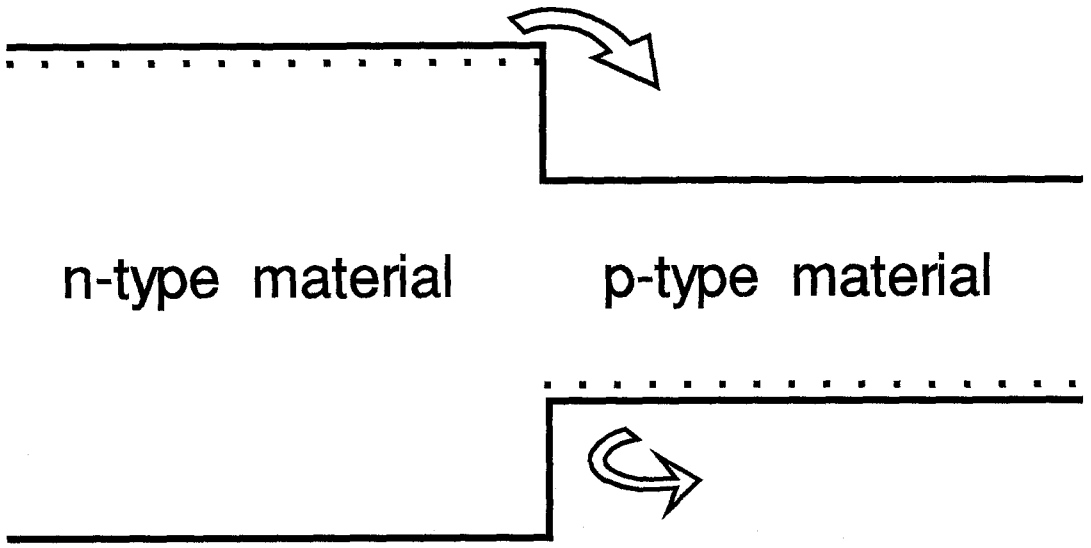

Figure 2.3: Flat band diagram of an ideal type-I heterojunction for efficient minority carrier injection. In this case a wider band gap n-type material achieves efficient electron injection into the recombination p-type material. The holes from the p-type material are blocked by the valence band offset, and the electrons see no barrier to injection.

since a large band gap material will have either a high conduction band or low valence band.

An ideal heterojunction for efficient minority carrier injection would have a type-I band offset for a given recombination material as shown in figure 2.3. We notice that in this ideal case there would be no barrier for electron injection into the p-region, but the valence band offset would block holes. This band alignment is the same principle used in long wavelength single and double heterostructure LEDs and LD where amphoteric lattice-matched ternery and quaternary alloys are used for both p and n materials. Unfortunately a natural heterojunction system for a type-I band alignment doesn't exist in the II-VI materials under the physical constraints present.

To realize a II-VI LED device based on a heterostructure, we must design a

structure given the material constraints of the II-VI semiconductors (doping and lattice constant) and engineer a solution to the unfavorable band offsets.

2.3 n-CdSe/p-ZnTe heterojunction

On close examination of figure 2.2, we note that CdSe and ZnTe are the only closely lattice matched (0.4% mismatch) heterojunction pair among the II-VI binary compounds. Furthermore, the two compounds can form a p-n heterojunction relying only on the natural doping proclivities for these materials. Although CdSe does not exhibit a stable zinc blende phase when grown in the bulk, prefering instead the wurzite structure, high quality epitaxial layers of zinc blende CdSe can be grown by MBE on (100) zinc blende substrates [16] and epilayers of ZnTe [17]. With the slight lattice mismatch between the cubic lattice constants, several hundred angstroms of CdSe can easily be grown on ZnTe without exceeding the critical thickness. Given this we might expect the n-CdSe/p-ZnTe heterojunction to form the basis of a wide band gap II-VI heterojunction LED.

Figure 2.4 shows a flatband diagram of an abrupt n-CdSe/p-ZnTe heterojuction. Unfortunately this heterojunction has a type-II band alignment, with the valence band of CdSe lying 0.64 eV below that of ZnTe and the conduction band of CdSe lying 1.22 eV below that of ZnTe [18]. The valence band offset provides a desired barrier to hole injection into the CdSe, but the larger conduction band offset serves as a greater barrier to electron injection. Under forward bias, both electrons and holes see large energy barriers at the heterojunction interface. As a result of this we would expect insignificant thermionic emission and mostly non-radiative recombination.

Computer simulations and attempts at fabricating a n-CdSe/p-ZnTe heterojunction confirm this suspicion. Figure 2.5 shows the band edge profile and carrier concentrations for an abrupt heterojunction under a forward bias of 1.25 volts calculated using the drift-diffusion model of Wang *et al.* [19].

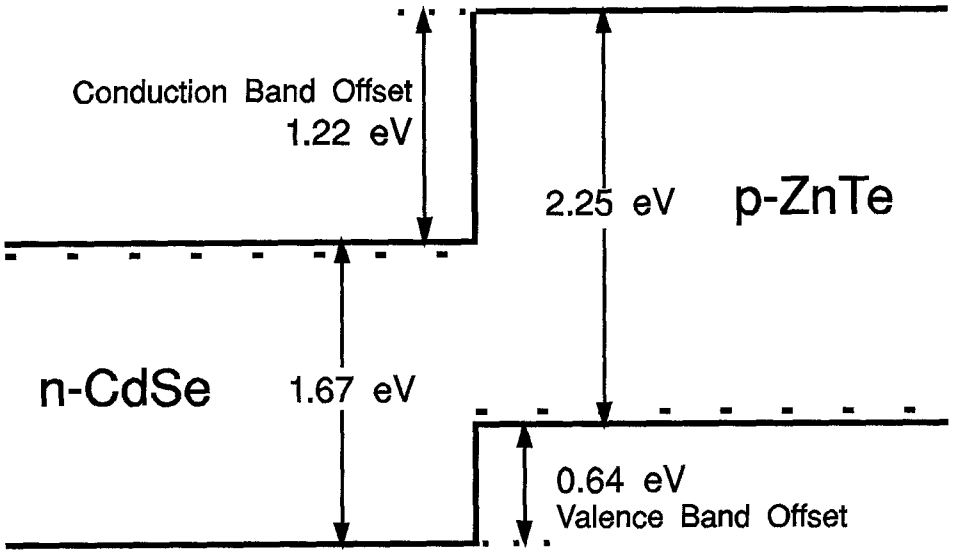

Figure 2.4: Flat band diagram of the only closely lattice-matched binary II-VI compounds. The resulting p-n heterojunction has a type-II band alignment. There exists the favorable condition that the valence band offset blocks the extraction of holes from the ZnTe. Unfortunately, the larger conduction band offset serves as a barrier to electron injection into the ZnTe.

As expected, the device simulations show carrier accumulation at the interface and virtually no carrier injection across the junction. The resulting overlapping carrier accumulation leads to predominantly non-radiative interfacial recombination. At larger biases some hole injection into the CdSe may occur but negligible electron injection is seen due to the larger conduction band barrier. Therefore, the simulations corroborate our intuition and demonstrate the futility of an abrubt n-CdSe/p-ZnTe heterojunction as a light emitter.

We could use these two binaries to form a quaternary alloy, $(CdSe)_{1-x}(ZnTe)_x$, which could be used as an intermediary layer between the n-CdSe and p-ZnTe. In principle, we could grade the band edges continuously from ZnTe to CdSe by varying x from 1 to 0 in the quaternary alloy $(CdSe)_{1-x}(ZnTe)_x$. This would eliminate the abrupt interface and carrier accumulations but the resulting current

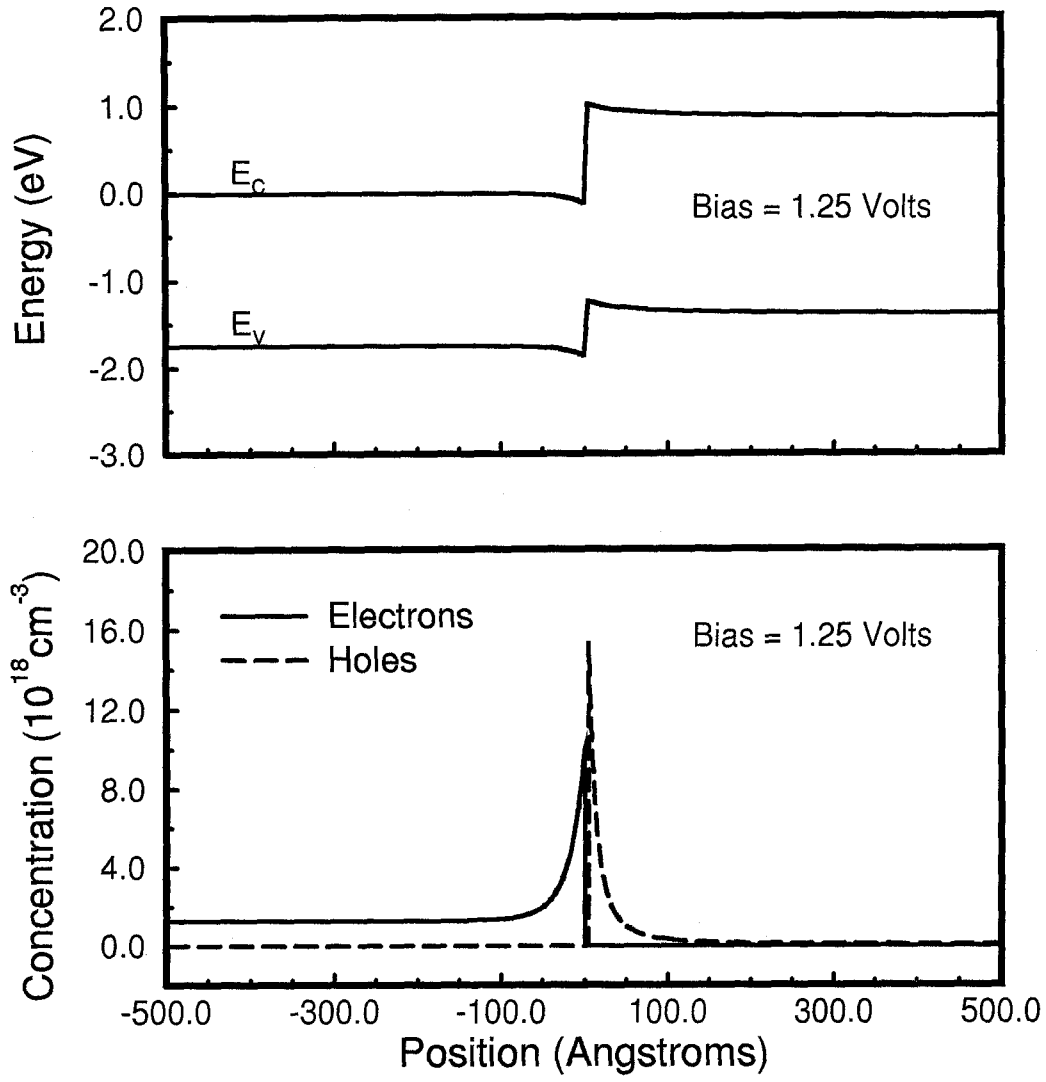

Figure 2.5: Calculated band bending and carrier concentrations for an abrupt n-CdSe/p-ZnTe heterojunction. The computer simulation is based on the drift-diffusion model of Wang *et al.* [19]. Both valence and conduction band barriers lead to overlapping carrier accumulation at the interface and non-radiative recombination.

would be predominantly hole injection into the CdSe due to the much smaller effective barrier in the valence band.

2.4 $Mg_xCd_{1-x}Se$ graded junction

Although an abrupt heterojunction will not suffice for a light emitter, the n-CdSe and p-ZnTe system can still be used to realize a p-n heterojunction LED. The graded injector device is based on the favorable properties of these two compounds, namely the natural doping type for these materials and the valence band offset. To facilitate electron injection from the n-CdSe into the p-ZnTe, while preventing hole extraction, we must grade the conduction band (CB) continuously from the CdSe CB to the ZnTe CB in an intermediary junction region, while maintaining the abrupt valence band offset. Since the anion of the II-VI materials predominantly determines the valence band edge position, this junction grading can be accomplished by alloying CdSe with an appropriately chosen wider band gap selenide.

The McCaldin diagram in figure 2.6 shows the properties of an expanded group of II-VI materials including the magnesium chalcogenides. We see the Mg-chalcogenides have very large band gaps and can be alloyed with the Zn and Cd compounds to increase the band gap. Unfortunately, there is no lattice matched ternary II-VI analogous to the III-V $Al_xGa_{1-x}As$ system. Therefore any introduction of Mg in a II-VI ternary will be associated with a lattice strain.

We observe in the McCaldin diagram of figure 2.6 that an alloy of $Mg_xCd_{1-x}Se$ can be formed which will have a zero conduction band offset and a large valence band offset with ZnTe. The graded injector device first proposed by Phillips *et al.* [20] is based on using an alloy of $Mg_xCd_{1-x}Se$ to continously grade the conduction band from ZnTe to CdSe, at the same time maintaining the valence band offset. The schematic in figure 2.7 illustrates a flatband diagram for the idealized graded injector device resulting from this band edge engineering. Starting from

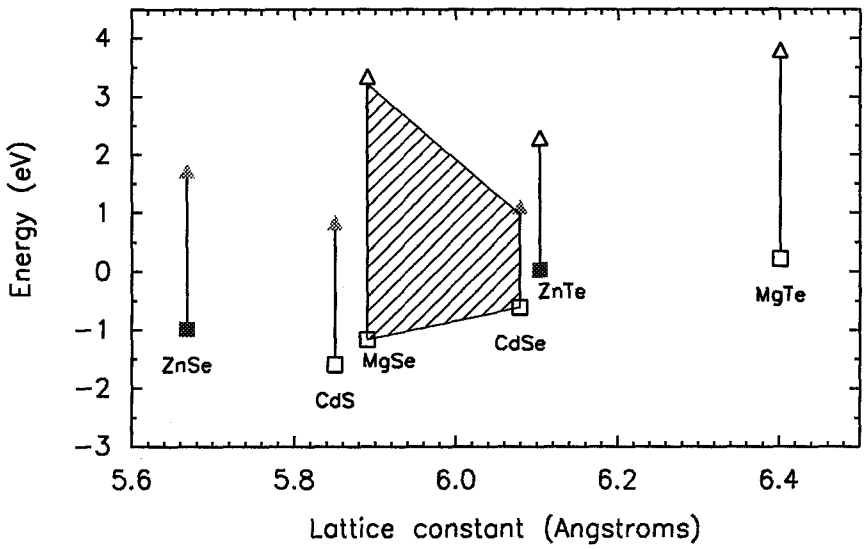

Figure 2.6: McCaldin diagram of common II-VI materials and the Mg-chalcogenides. The $Mg_xCd_{1-x}Se$ ternary alloy is represented by the shaded region. The band gap of MgSe is the estimated value derived in Chapter 4 of this thesis. The band offsets of MgSe and MgTe are from Wang *et al.* [21]. The band gap of MgTe is from Parker *et al.* [22] and the lattice constant is from Waag *et al.* [23]. The lattice constant of MgSe is from Okuyama *et al.* [24], as are the band gap and lattice constant of MgS. The band offset for MgS assumes the common anion rule, which states that the position of the valence band edge is determined by the constituent anion. The band gaps and lattice constants for the Mg-Chalcogenides are extrapolated values for the zinc blende structure. We notice that for a specific alloy of $Mg_xCd_{1-x}Se$ there can a zero conduction band offset with ZnTe.

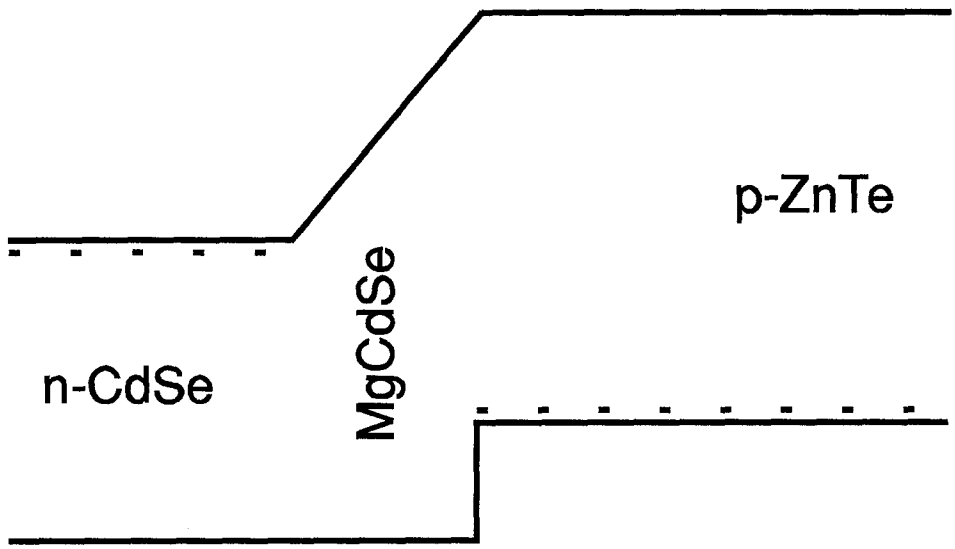

Figure 2.7: Flatband diagram of an n-CdSe/$Mg_xCd_{1-x}Se$/p-ZnTe heterojunction. This "graded junction" device facilitates electron injection while preserving the valence band offset to confine the holes. Beginning at the $Mg_xCd_{1-x}Se$/ZnTe interface we grade the Mg concentration until we have only CdSe. This schematic assumes the common anion rule for the valence band offset, although the valence band of $Mg_xCd_{1-x}Se$ is lowered with increasing Mg concentration. The initial Mg concentration will depend on the band gap and valence band position of the $Mg_xCd_{1-x}Se$ alloy.

the $Mg_xCd_{1-x}Se$/ZnTe interface we grade the Mg concentration from some specific amount down to CdSe over a few hundred angstroms.

To properly grade the alloy to the conduction band of ZnTe we must know the band gap and band offset for $Mg_xCd_{1-x}Se$ as a function of Mg concentration. There is a large variation in the estimates and extrapolations of the band gap of MgSe ranging from 3.6 to 5.6 eV [24, 25]. Furthermore, the effect on the valence band edge with the addition of Mg was previously unknown. In chapter 4, we investigate these materials' properties to best determine the alloy concentration needed for a zero conduction band offset between $Mg_xCd_{1-x}Se$ and ZnTe. We find

a good estimate for the maximum Mg concentration to be about 69%.

The lattice constant of zinc blende MgSe has an extrapolated value of 5.89 Å [24], therefore the introduction of Mg into CdSe will introduce a fairly large lattice strain with respect to ZnTe. For the estimated maximum Mg concentration, the mismatch to ZnTe will be 2.4%. This is a large lattice strain to accommodate, but since the Mg concentration is graded down to CdSe it is only the peak strain. Therefore if we can keep the alloy junction region thin enough we should be able to stay below the critical thickness. We lack any accurate ability to calculate the critical thickness for this given structure but we estimate that the thickness of the whole graded region must be less than 300 Å [20]. Device simulations demonstrate that the grading can be very thin and still operate as expected [19].

To better understand the role the graded junction plays in the device operation and the mechanism by which the graded device works we can look at the drift-diffusion simulation results of Wang *et al.* [19]. Figure 2.8 shows the resulting band edge profile and carrier concentrations for a $Mg_xCd_{1-x}Se$ graded junction device under a 2.0 Volt forward bias. These results where calculated for a 200 Å graded region. As the thickness becomes much thinner the injection efficiency begins to decrease, but if the thickness becomes too large we will have to be concerned with exceeding the critical thickness and defect formation. Simulation results also demonstrate that the operation of the graded junction does not require the graded region to be doped.

We note two significant differences in this device operation compared to the abrupt heterojunction in figure 2.5. First, we see the graded region effectively reducing the barrier in the conduction band and preserving the barrier in the valence band. And secondly, we notice that the graded junction spatially separates the accumulation of electrons and holes. As long as this separation distance is roughly larger than the Bohr radius of an exciton, there should be no significant overlap of the electron and hole wavefunctions and therefore a dramatic reduction in the non-radiative recombination due to the accumulation. The net effect of the

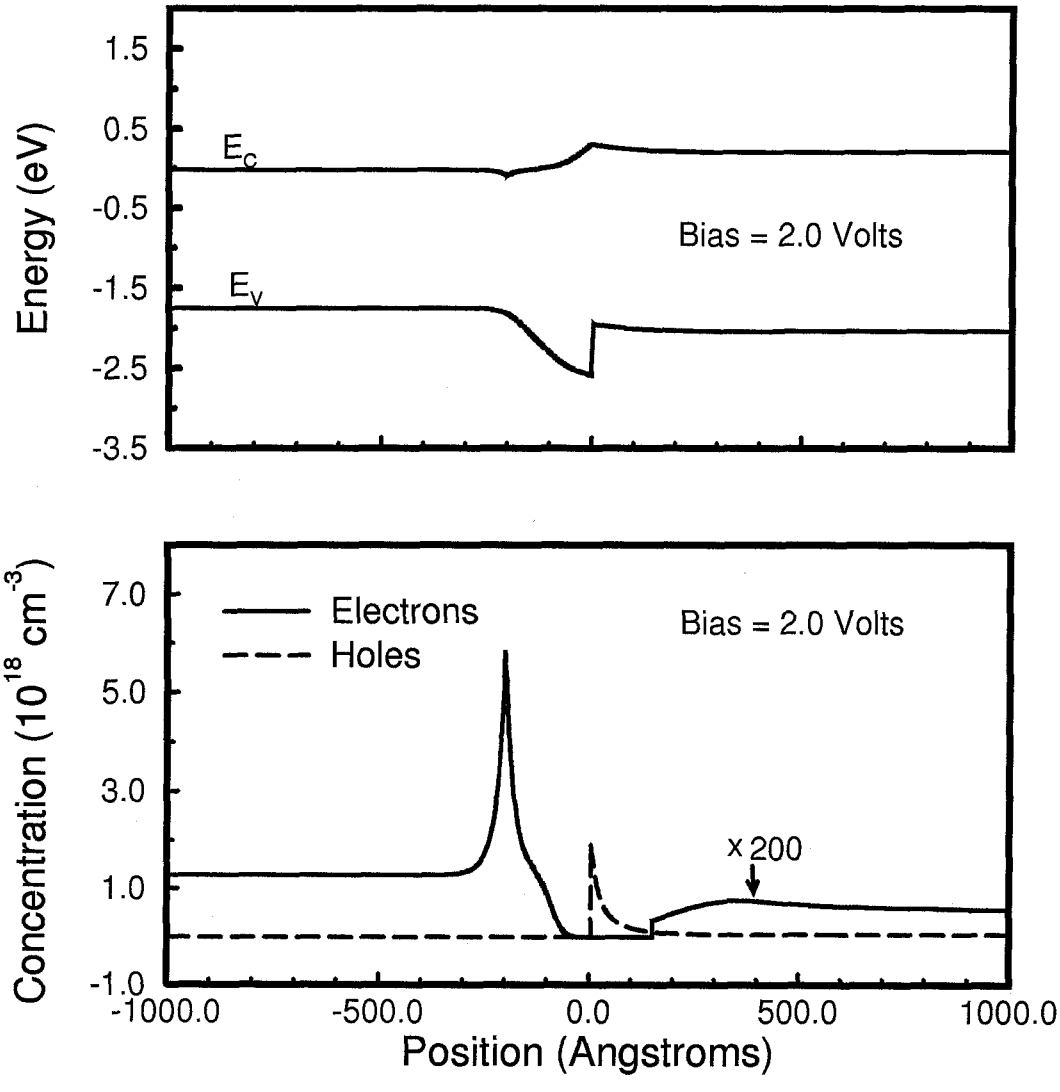

Figure 2.8: Calculated band edge profile and carrier concentrations under a forward bias of 2.0 Volts. The simulated results are based on the drift-diffusion model as calculated by Wang *et al.* [19]. This model used a graded region 200 Å thick. Notice the reduced barrier for electrons compared to the abrupt heterojunction in figure 2.5, as well as the spatial separation of the charge carriers. We are beginning to see the onset of minority carrier injection into the ZnTe.

graded region is to facilitate electron injection into the wider band gap ZnTe. At low bias voltage, most of the current is non-radiative interfacial recombination. But as the bias is increased, we begin to see significant electron injection into the ZnTe where they can recombine radiatively. Since the large valence band offset remains, there is no hole extraction into the CdSe.

The early device results were severly limited by the lack of a p-type dopant for MBE grown ZnTe and the use of poor quality ZnTe substrates [20]. In spite of these restrictions, early devices worked as light emitting devices with light emission originating from the ZnTe substrate. Unfortunately though, these devices operated at high bias voltages and therefore the injection mechanism was not thoroughly understood. It was unclear whether the devices operated as high field effect devices rather than normal thermionic p-n junction diodes. Work on materials and device development covered in the following chapters of this thesis led to the fabrication of graded junction LEDs which unequivocally demonstrate the diode like operation as predicted by the simulations.

2.5 Conclusion

A novel p-n heterojunction LED based on the only closely lattice matched II-VI binary pair (n-CdSe/p-ZnTe) is demonstrated to be capable of minority carrier injection. Although an abrupt n-CdSe/p-ZnTe heterojunction results in non-radiative currents, an efficient electron injector is created by engineering the band edges with an intermediary $Mg_xCd_{1-x}Se$ alloy junction region.

Bibliography

[1] For a discussion of the physics of p-n junctions, see A. S. Grove, *Physics and Technology of Semiconductor Devices* (Wiley, New York, 1967), pp. 149-207.

[2] H. Kressel, *Semiconductor Lasers and Heterojunction LEDs* (Academic Press, New York, 1977).

[3] K. Ohkawa, T. Mitsuyu and O. Yamazaki, *J. Cryst. Growth* **86**, 329, (1988).

[4] R. Park, M. Troffer, C. Rouleau, J. DePuydt and M. Haase, *Appl. Phys. Lett.* **57**, 2127, (1990).

[5] J.O. McCaldin, *J. Vac. Sci. Technol. A* **8**, 1188 (1990).

[6] W.A. Harrison, *J. Vac. Sci. Technol.* **14**, 1016 (1977).

[7] E.T. Yu, J.O. McCaldin and T.C. McGill, *Solid State Physics*,v. **46**, (Academic Press, 1992).

[8] M. Aven and W. Garwacki, *Appl. Phys. Lett.* **5**, 160, (1964).

[9] M.V. Kot, L.M. Panasyuk, A.V. Simashkevich, A.E. Tsurkan and D.A. Sherban, *Sov. Phys.-Solid State* **7**, 1001, (1965).

[10] S. Fujita, S. Arai, F. Itoh and T. Sakaguchi, *J. Appl. Phys.* **46**, 3070, (1975).

[11] J.O. McCaldin and T.C. McGill, *J. Vac. Sci. Technol. B* **6**, 1360, (1988).

[12] E.T. Yu, E.T. Crooke, D. H. Chow, D. A. Collins, M.C. Phillips and T.C. McGill, *J. Vac. Sci. Technol. B* **8**, 908, (1990).

[13] J. Han, T.S. Stravrinides, M. Kobayashi, R.L. Gunshor, M.M. Hagerott and A.V. Nurmikko, *J. Elec. Mater.* **22**, 485, (1993).

[14] S.Y. Ren, J.D. Dow and J. Shen, *Phys. Rev. B* **38**, 10677, (1988).

[15] J.D. Dow, R.D. Hong, S. Klemm, S.Y. Ren, M.H. Tsai, O.F. Sankey and R.V. Kasowski, *Phys. Rev. B* **43**, 4396, (1991).

[16] N. Samarth, H. Luo, J. Furdyna, S. Qadri, Y. Lee, A. Ramdas and N. Otsuka, *J. Elec. Mater.* **19**, 543, (1989).

[17] H. Luo, N. Samarth, F. Zhang, A. Pareek, M. Dobrowolska, J. Furdyna, K. Mahalingam, N. Otsuka, W. Chou, A. Petrou and S. Qadri, *Appl. Phys. Lett.* **58**, 1783, (1991).

[18] E. Yu, M. Phillips, J. McCaldin and T. McGill, *J. Vac. Sci. Technol. B* **9**, 2233, (1991).

[19] M. Wang, M. Phillips, J. Swenberg, E. Yu, J. McCaldin and T. McGill, *J. Appl. Phys.* **73**, 4460, (1993).

[20] M. Phillips, M. Wang, J. Swenberg, J. McCaldin and T. McGill, *Appl. Phys. Lett.* **61**, 1962, (1992).

[21] M. Wang, J. Swenberg, M. Phillips, E. Yu, J. McCaldin R. Grant and T. McGill, *Appl. Phys. Lett.* **64**, 3455, (1994).

[22] S. Parker, A. Reinberg, J. Pinnell and W. Holton, *J. Electrochem. Soc.* **118**, 979, (1971).

[23] A. Waag, H. Heinke, S. Scholl, C. Becker and G. Landwehr, *J. Cryst. Growth* **131**, 607, (1993).

[24] H. Okuyama, K. Nakano, T. Miyajima and K. Akimoto, *Jpn. J. Appl. Phys.* **30**, L1620, (1991).

[25] W. Strehlow and E. Cook, *J. Phys. C* **2**, 163, (1973).

Chapter 3

Molecular Beam Epitaxy, and Nitrogen Doping of ZnTe

3.1 Introduction

Molecular beam epitaxy (MBE) offers a number of advantages as a crystal growth technology for the growth of II-VI compounds and the graded injector device structure. Elemental and/or compound source materials with purities of 99.99999% or greater are available. The ultra-high vacuum (UHV) growth condition of MBE enables the growth of layers with very high purity as well as allowing for *in situ* growth analysis. A residual gas analyzer (RGA) detects the constituent atomic and/or molecular species in the UHV environment. Reflection high energy electron diffraction (RHEED) provides surface analysis of epitaxial films during MBE growth. The low growth temperatures, as low as 150 °C for ZnSe, and the precise monolayer control of beam fluxes enable the formation and control of abrupt heterojunction interfaces with interdiffusion and reactions between III-V/II-VI or II-VI/II-VI junctions limited to a few atomic layers. MBE is well suited for growth of the graded injector device not only for its material purity and low temperature growth, but also for its thickness and compositional control which are necessary

for our device structure. Other techniques, such as metal organic chemical vapor deposition (MOCVD), are capable of the low temperature epitaxial growth but they require more understanding and control of the chemical reactions and gas flows. Furthermore MBE is considerably safe when compared to MOCVD, which can require the use of toxic gas sources.

One common problem with the growth of II-VI semiconductors has been the unavailability of high quality substrates. This problem is partially mitigated by using lattice matched III-V substrates, which are commercially available and of high structural quality. For instance, for the growth of ZnTe we can use GaSb substrates with a lattice mismatch of 0.128%. There are two subtle, yet noticeable problems associated with this approach. First, there is measureable cross contamination due to the out-diffusion of group III and V elements. Second, there are interfacial chemical reactions at the III-V/II-VI heterojunction.

Since the constituent atoms of a III-V compound are dopants in II-VI materials the substrate elements can diffuse out of the III-V layer and into the II-VI material during growth. This will result in doping compensation and the formation of impurity states. Rajakarunanayake *et al.* [1] found the out-diffusion of group III and group V impurities in the growth of epilayers of ZnTe on various III-V substrates. Photoluminescence (PL) from the ZnTe exhibited characteristic impurity bound excitons due to the cation out-diffusion. Secondary-ion mass spectroscopy and electron microprobe analysis showed substantial out-diffusion of the III-V cations and anions into the ZnTe with higher concentrations at the surface of the ZnTe than in the epilayer. It was also seen that there was no significant back diffusion of Te into the III-V layers. In our studies of ZnTe growth on GaSb substrates we observed significant Sb out-diffusion, detected by XPS, with roughly a monolayer of Sb riding up along the growth surface. This isn't surprising since Sb is known to be and is used as a surfactant during MBE growth [2, 3]. Although out-diffusion is not ideal, it can be somewhat reduced and tolerated so long as it doesn't prevent doping or hinder the II-VI epilayer structural quality.

A more severe consequence of II-VI/III-V heteroepitaxy is the formation of interface compounds. Tu and Kahn [4] observed the formation of an interfacial layer (~5 Å) between ZnSe and GaAs during MBE, which was later determined by XPS to be Ga_2Se_3 [5]. A similar interfacial reaction was found for the ZnTe/GaSb heterojunction. XPS [6], raman scattering [7] and high resolution electron microscopy [8] confirmed the formation of Ga_2Te_3 at the ZnTe/GaSb interface during MBE growth. Duddles *et al.* [9] found an anomalous blue shift of the heavy-hole exciton that could not be explained by the lattice mismatch between ZnTe and GaSb. They suggested that the interfacial Ga_2Te_3 contributed to additional strain. We find the presence of this interfacial III-VI layer degrades the subsequent layer quality.

Petruzzello *et al.* [10] found that the structural quality of ZnSe grown on GaAs was strongly dependent on the specific growth initiation. With an initial exposure of Zn-only prior to growth initiation, the interface layer and epitaxial film was of high structural quality. On the other hand, an initial exposure of Se resulted in films of significantly lower quality. This demonstrated not only that the interface compound layer affects the epitaxial growth quality, but also that it may be possible to control the degree of its effect.

3.2 Overview and outline

Our MBE system consists of three separate chambers, interconnected via UHV transfer tubes. Two of the chambers are Perkin-Elmer 430P MBE systems, one dedicated to III-V only and the other to II-VI only growths. The third chamber is a Perkin-Elmer Model 5500 analysis system used for x-ray photoelectron spectroscopy (XPS). Elemental source materials are used in conventional MBE ovens. The base pressures in the chambers during growth or analysis are typically in the low 10^{-10} Torr range, although during nitrogen doping the pressures are as high as 10^{-6} Torr. Typical substrate growth temperatures during II-VI growth are 300 °C,

and fluxes are set for growth rates of ~ 1 Å per second. Optimal MBE growth of ZnTe was found to occur for a flux ratio of Zn to Te which is slightly "Te-rich" and exhibiting the characteristic (2×1) RHEED reconstruction. The transfer tubes allow for sample manipulation between the separate chambers without removing from the UHV (10^{-10} Torr) environment. By interconnecting these different chambers we are capable of growing II-VI/III-V heteroepitaxial samples as well as offering additional *in situ* (XPS) materials characterization, while avoiding cross chamber contamination.

Early attempts at fabricating a graded injector LED based on the graded injector heterojunction were severely limited by the lack of high quality ZnTe substrates. Before the successful p-type doping of MBE ZnTe, the early devices had to be grown on poor quality p-ZnTe, and we had to rely on the p-typeness of the substrate with only a thin buffer layer for device operation. With the success of p-type doping of ZnTe, detailed in this chapter, we could then grow high conductivity layers of p-ZnTe and use the closely lattice matched GaSb as a substrate. Although GaSb substrates offer a partial solution to the substrate deficiency, we found it necessary to control the II-VI/III-V interfacial reaction. By using a thin intermediary AlSb buffer we could suppress the II-VI/III-V interfacial reaction and grow considerably higher quality ZnTe epilayers.

In this chapter we discuss the issues and details of the growth technologies used to fabricate the graded injector LED. A discussion of the substrates used for MBE growth is presented with the emphasis on the ability to use commercially available GaSb. In addition, nitrogen doping of ZnTe is presented along with the technique used to achieve high quality epilayers with adequate doping levels necessary for device operations. Lastly the growth technique employed to construct the $Mg_xCd_{1-x}Se$ graded region is discussed and evaluated.

3.3 Substrate choice

3.3.1 ZnTe

Ideally, we would prefer homoepitaxy over heteroepitaxy to avoid interfacial reactions and any residual strain. Unfortunately, high quality ZnTe substrates have not been available. Single-crystal ZnTe substrate were obtained from Eagle-Picher [11]. A proprietary seeding technique was used to nucleate crystal growth on a substrate and bulk substrate growth proceeded via a physical-vapor-transport. Crystalline quality has varied, with x-ray FWHM ranging from 70-110 arcsecs. Polishing and surface preparation technology has not been as advanced as for the III-V semiconductors, and polish damage was visually apparent on the ZnTe substrates. Furthermore, substrate preparation and deoxidation of ZnTe substrates has been a considerable problem. We have been unsuccessful in desorbing oxygen bound to Zn on the surface. This residual surface oxide nucleates twins during growth. Ar ion sputtering can remove the surface oxide, but the sputtering damage also leads to growth defects nucleating at the defect sites on the surface. Annealing the substrates at 460 °C prior to growth improves the surface structure, as seen in the RHEED pattern. This annealing step was found to lead to better growth nucleation than the unsputtered substrates so all growths on ZnTe are sputtered and annealed. In spite of this procedure, the surface morphology of thick epilayers of ZnTe grown on these ZnTe substrates is generally poor compared to high quality heteroepitaxy on GaSb. These thick layers on ZnTe substrates have much higher surface roughness than growths on GaSb, and exhibit hillock formation nucleating at the substrate/epilayer interface [12]. The electrical (J-V) and optical (electroluminescence and quantum efficiency) properties of devices grown on ZnTe substrates were greatly outperformed by comparable devices grown on GaSb. Therefore, ZnTe substrates were used primarily for growths of characterization epilayers rather than for devices, and GaSb substrates were used for device

growths.

3.3.2 GaSb

For lack of a homoepitaxial technique to ZnTe growth, GaSb offers an improved alternative for a substrate material. GaSb is a closely latticed match III-V binary substrate commercially available with reasonable quality. The ZnTe/GaSb lattice mismatch is 0.128%, which is better than that of ZnSe/GaAs (0.254%) and that of AlAs/GaAs (0.132%). GaSb substrates used have typical x-ray FWHM of 18 arcsec. High quality MBE GaSb is well established, so epilayers of GaSb can be grown for later II-VI epitaxy. These features make GaSb an ideal candidate substrate for II-VI ZnTe epitaxy. Additionally since we can now dope ZnTe *p*-type, GaSb can be a substrate for device applications. The valence band of ZnTe is 0.60 eV lower than the valence band of GaSb [13], so a *p*-type contact through the substrate is difficult. Fortunately, ohmic contacts to *p*-ZnTe can be made from the top side laterally to a device.and serve as a back contact.

Unfortunately, the interfacial reaction between ZnTe and GaSb forming Ga_2Te_3 can result in epilayers with high defect densities and poor structural and surface quality. Typical x-ray FWHM for epilayers of ZnTe on GaSb where > 100 arcsecs. The interface reaction appears to be slightly supressed by initiating growth with an initial Zn flux similar to the technique of Petruzzello *et al.* [10]. Since the Ga-Sb and Zn-Te bonds are respectively weaker than the Ga-As and Zn-Se bonds, this technique is less effective than with ZnSe growth on GaAs. A better technique employed is to grow a thin ($\sim$ 20 Å) buffer of AlSb on the GaSb epilayer. The AlSb has a stronger chemical bond and the formation of Al_2Te_3 at the AlSb/ZnTe interface is reduced. This result was observed in the RHEED pattern during the initial growth nucleation. For samples without the AlSb, the RHEED pattern becomes diffused immediately upon growth of ZnTe and then becomes slightly spotty and streaky after roughly 4-6 seconds. For samples with the AlSb, the

RHEED pattern is less diffused and slightly spotty at the onset of ZnTe growth. This at least qualitatively demonstrates a reduced interfacial reaction with the AlSb buffer. In addition, higher quality ZnTe epilayers where grown using an AlSb buffer. Best x-ray FWHM of 39 arcsec and typical x-ray FWHM of 40-50 arcsec were achieved using the AlSb buffer. Therefore, all II-VI growths on GaSb substrates had the thin AlSb buffer layer.

3.4 Nitrogen doping of ZnTe

Bulk grown ZnTe, grown with an excess of Te will be p-type due to the formation of the double acceptor Zn vacancy. We would expect ZnTe to be easily doped p-type by MBE, but there has been considerable difficulty achieving high quality p-type ZnTe. Undoped MBE-grown ZnTe is naturally p-type but highly resistive. During MBE growth, excess Zn or Te can re-evaporate from the surface resulting in stoichiometric material with high resistivity. A number of early attempts to dope ZnTe during MBE growth have had only limited success. Antimony doping has been limited both by low solubility and low activation efficiency, with maximum p-type carrier concentrations of $3\times10^{15}\text{cm}^{-3}$ achieved without degrading the films [14]. Elemental phosphorus doping with beam equivalent pressures comparable to the Zn and Te sources has attained carrier concentrations up to $4\times10^{17}\text{cm}^{-3}$, but with deteriorated crystalline quality [15]. More efficient p doping has been achieved using Zn_3As_2 for arsenic doping with hole concentrations up to $1\times10^{18}\text{cm}^{-3}$ [16]. But as with the phosphorus doping the beam equivalent pressure was greater than for the Zn and Te. More limiting, though, is the formation of deep levels for $p > 1\times10^{17}\text{cm}^{-3}$, and severely degraded band edge photoluminescence in favor of deep emission due to arsenic incorporation.

Recently, nitrogen has shown to be an effective p-type dopant in ZnSe [17]. Resistivities below 1 Ω-cm [18] have been grown, however net acceptor concentrations saturate at $2\times10^{18}\text{cm}^{-3}$ under optimal growth conditions for ZnSe [19]. Further

nitrogen incorporation can be increased to as high as 1.3×10^{19}cm^{-3}, but the net acceptor concentration does not increase due to compensation. The incorporation of nitrogen higher than 1×10^{18}cm^{-3} was further shown to affect the structural properties of ZnSe attributed to the formation of point defects accompanying the N doping [20].

The successful nitrogen doping has been accomplished by forming a nitrogen plasma. Most researchers have employed an Oxford Applied Research (OAR) [21] radio frequency (RF) plasma source. Another possible source studied has been an electron cyclotron resonance (ECR) plasma source [22]. Vaudo *et al.* [23] have investigated the optical emission spectra of both RF and ECR sources and identified atomic species in the nitrogen plasma as the most likely species responsible for *p*-type doping. Furthermore, it was shown that the RF source produces a larger percentage of nitrogen atoms for a given set of operating condition as well as doping to higher free hole concentrations than the ECR source. Therefore we suspect that an RF plasma source will be a preferred efficient atomic nitrogen source for *p*-type doping of II-VI compounds.

Soon after the accomplishment of *p*-type doping of ZnSe with a nitrogen plasma source, *p*-type doping of ZnTe was demonstrated. Han *et al.* [24] grew ZnTe:N epilayers on (100) GaAs susbstrates with acceptor concentrations approximately 1×10^{19}cm^{-3} and x-ray FWHM of 270 arcsec. We successfully doped ZnTe grown on ZnTe substrates using a nitrogen plasma source with hall carrier concentrations up to 1×10^{20}cm^{-3} [25]. Tao *et al.* [26] also acheived doping levels of 1×10^{20}cm^{-3} in ZnTe by growing on tilted (311)B GaAs substrates. On (100) GaAs substrates they measured hole concentrations of 8.9×10^{19}cm^{-3} under identical growth conditions. The successful doping of ZnTe to these levels has facilitated the fabrication of low resistance "pseudograded band gap" contacts to *p*-ZnSe formed with a ohmic contact to ZnTe:N graded with Zn(Se,Te):N to ZnSe:N [27]. Additionally, *p*-type ZnTe has led to significant advancements in the development of the "graded injector" [25] visible light emitter discussed later in this thesis.

3.4.1 Nitrogen plasma source

Nitrogen doping is achieved by using an OAR Atom/Radical-Beam Source, Model MPD21. This source fits in the standard effusion cell of the MBE machine. A Nanochem Series L-60 gas purifier with Nanochem 1400 resin is used to reduce any impurities of 0_2, H_20, and $C0_2$ in the gas source to the ppb (parts per billion) levels. The gas flow rate is set with a precision needle valve. A plasma is struck in the PBN (pyrolytic boron nitride) discharge tube by an electrical discharge created from inductively-coupled RF excitation at 13.56 MHz. Atomic and radical species produced in the discharge can escape into the vacuum chamber via an array of fine holes in the beam aperture plate. Two apertures with different number of pin holes and pin hole diameters have been used in our system: a 21 x 0.3mm (number x diameter) array with an effective area of 1.48 mm^2, and a 4 x 0.2mm array with an effective area of 0.13 mm^2. The size and number of holes in the aperture sets the aperture conductance and therefore controls the beam flux and flow rates necessary for plasma discharge. For instance, with the larger array a N_2 flow > 0.05 sccm is necessary for plasma operation, while with the smaller array a N_2 flow ≥ 0.01 sccm is needed [28]. As will be shown below the smaller array was used to reduce the dopant flux.

3.4.2 Nitrogen doping of ZnTe

An ultra high purity (99.9995%) nitrogen gas source was used in our early doping experiments. The major impurity Ar, which is inert, had levels $<$ 5 ppm (parts per million). Other contaminants are effectively reduced by the Nanochem purifier. The plasma source had the 21 x 0.3mm aperture installed. The nitrogen flow rate was adjusted for these experiments to yield a background chamber pressure of 1×10^{-6} Torr, and the plasma was operated at 125W with no reflected power.

Epilayers of nitrogen doped ZnTe were grown on (100) ZnTe substrates to study the electrical characteristics of ZnTe:N. Growth conditions were typical for MBE

ZnTe epilayers previously discussed. The nitrogen doped layers were each grown to approximately 2 μm after the growth of roughly 1 μm of undoped ZnTe. The electrical properties of the ZnTe epilayers were evaluated by Hall measurements. Dopant concentrations in all experiments were sufficiently high to form ohmic contacts with all metals and contacts used (Au, Au/Ge, silver paint and indium solder).

Doped layers of ZnTe:N grown under these conditions were extremely conductive with resistivities of 10^{-3} Ω-cm, and hole carrier concentrations of 1×10^{20}cm^{-3}. We were unable to significantly reduce the nitrogen beam flux, while maintaining a plasma, for the given nitrogen source aperture. Therefore, to reduce the average doping concentration, we modulated the doping in a superlattice type fashion by repeatedly growing periods of undoped ZnTe followed by doped ZnTe:N. Figure 3.1 shows the results of Hall measurements of three different epilayers all grown to roughly the same thickness: one continously doped ZnTe:N, and two different modulated doped layers. One modulated doped layer has 40 periods of 500 Å ZnTe/50 Å ZnTe:N. The other modulated doped layer has 40 periods of 500 Å ZnTe/25 Å ZnTe:N. The lack of any temperature dependence is characteristic of fully degenerately doped material. In this regime, wave functions of N acceptor holes overlap and an impurity band is formed.

The modulated doping effectively reduces the average carrier concentration and increases the resistivities of the epilayers by up to 2 orders of magnitude. More importantly, the modulated doping improved the surface morphology of the ZnTe epilayers. The surface crystallinity was examined during growth by *in situ* RHEED. The RHEED shows the distinct (2 $\times$ 1) streaky "Te-rich" pattern characteristic of normal two-dimensional ZnTe growth. In the case of the continous doping, an elonged (2 $\times$ 1) spotty pattern developes as the layer grows indicating three-dimensional growth and degraded surface morphology. On the other hand, in the case of the modulated doping, the RHEED stays streaky and the surface morphology is improved over the continous doped case. This improvement is quantified

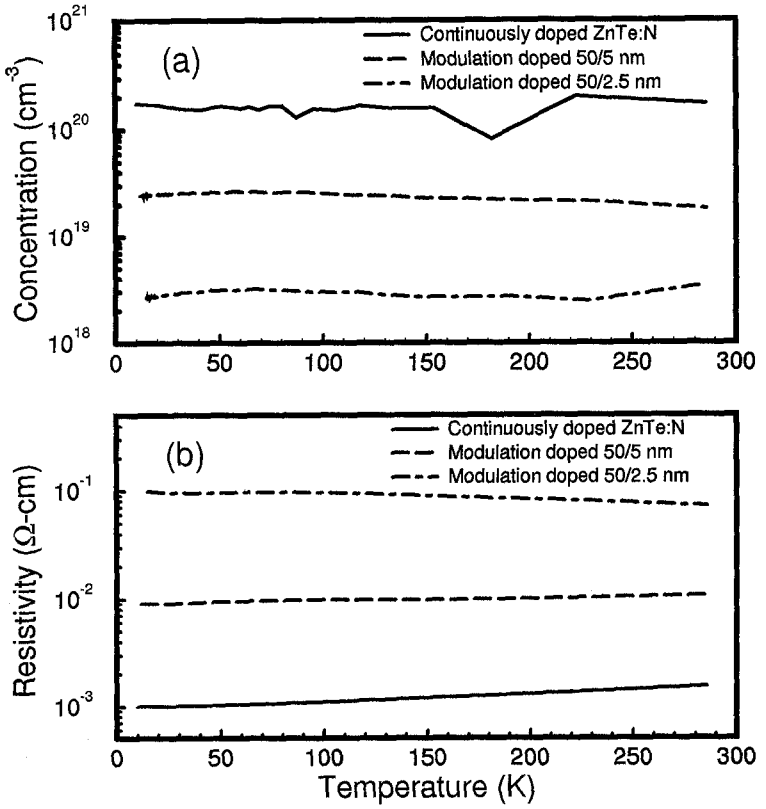

Figure 3.1: Hall measurement of nitrogen doped ZnTe epilayers as a function of temperature for (a) carrier concentration and (b) resistivity [29]. The 40 period modulated doped period thicknesses are given as undoped/doped in nanometers. All epilayers are roughly 2 microns of doped material grown on 1 micron undoped insulating ZnTe buffer layers.

by atomic force microscopy (AFM) and average root mean square (RMS) surface roughness [12]. These structural improvement results are very similar to planar doping techniques employed with chlorine doping of ZnSe by MBE [30].

The structural and growth problems associated with these degenerate doping levels may in large part be due to the large lattice strain associated with nitrogen incoporation. Nitrogen p-type doping is substitutional on a Te site. At the doping incorporation levels in these experiments, $1 \times 10^{20} \mathrm{cm}^{-3}$, roughly 0.5% of the Te sites are substituted with N. The tetrahedral radii of N is 0.70 Å while that of Te is 1.32 Å

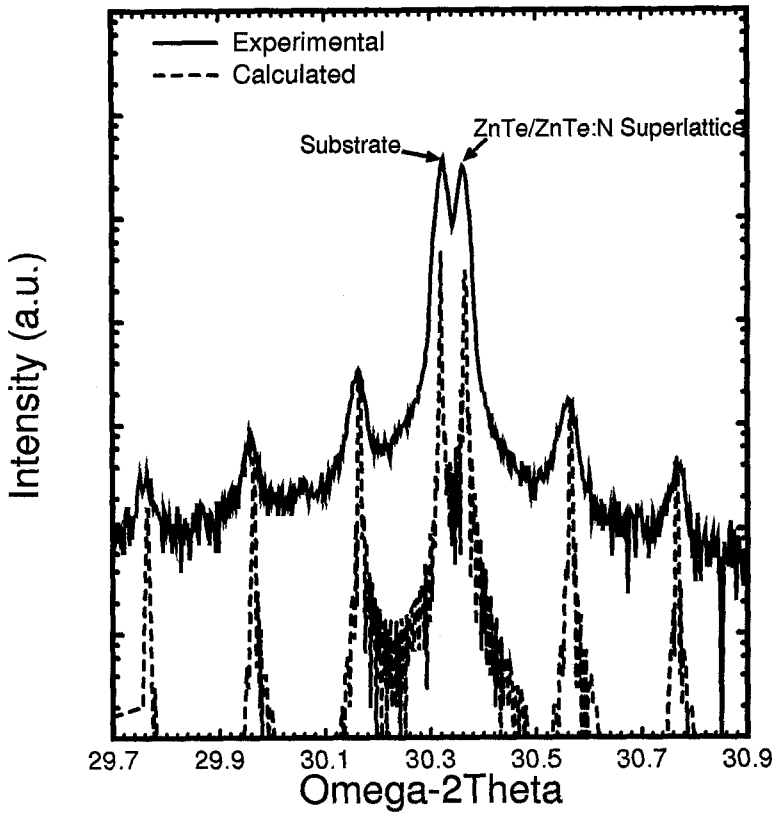

Figure 3.2: $\Omega/2\ \theta$ measured and calculated x-ray diffraction patterns for a 40 period ZnTe(240 Å)/ZnTe:N(15 Å) layer grown on ZnTe. Calculated pattern is generated by Philips PC-HRS software [32]. The lattice parameter for ZnTe:N is estimated using the tetrahedral radii of nitrogen and the doping concentration.

[31]. Therefore the doping will lead to large local strains. Figure 3.2 illustrates this effect. The X-ray diffraction for a modulated doped layer with 40 periods of 240 Å ZnTe/15 Å ZnTe:N doped to $1\times10^{20}\text{cm}^{-3}$ grown on ZnTe substrates is compared to a calculated diffraction pattern. A superlattice-like x-ray pattern is observed due to the periodic lattice strain due to the nitrogen doping.

Graded device structures were grown using the modulated N-doped ZnTe on GaSb substrates. These devices operated successfully as discussed in the following chapter, but due to the degenerate doping the optical performance was degraded. Photoluminescence from modulated doped ZnTe:N was less efficient than for un-

doped ZnTe. Therefore, it was necessary to reduce the doping levels significantly to improve the structural and optical quality of the ZnTe:N.

To reduce the doping levels the aperture on the nitrogen source was changed to the 4 x 0.2mm aperture. The effective area of this aperture is one order of magnitude smaller than the 21 x 0.3mm aperture, thus reducing the flux equivalently. Continuously doped epilayers of ZnTe:N, grown under similar growth conditions as mentioned above, had room temperature Hall hole carrier concentrations reduced to $2\times10^{19}\text{cm}^{-3}$. These layers showed improved photoluminesce over the higher doped layers but were still degraded as compared to undoped ZnTe layers.

3.4.3 Dilute nitrogen doping of ZnTe

To further improve the structural quality of the ZnTe:N we reduced the doping levels by changing the nitrogen gas source to an ultra high purity (99.9995%) dilute mixture of 10% N_2 / 90% Ar. The plasma could be struck with a similar gas flow rate and background chamber pressure. Therefore the nitrogen flux is effectively reduced by one order of magnitude. Continously doped epilayers of ZnTe:N grown using the dilute nitrogen and 4 x 0.2mm aperture under the above growth conditions had room temperature Hall hole carrier concentrations of $1\times10^{18}\text{cm}^{-3}$. These levels proved sufficient for ohmic contacting and epilayer conductivity. Furthermore, these ZnTe:N layers exhibited greatly improved photoluminescence over the higher doped layers and had PL comparable to undoped ZnTe layers. In addition, the structural quality of the ZnTe:N films grown under these conditions were as good as undoped epilayers. Figure 3.3 shows the x-ray rocking curve for an epilayer of ZnTe:N grown on a GaSb substrate with an intermediary 20 Å AlSb layer. This ZnTe:N epilayer had the best x-ray FWHM of 39 arcsec for all ZnTe growths on GaSb substrates. Therefore for optimal doping and materials quality we used the dilute N_2 source with the smallest aperture for subsequent device growths.

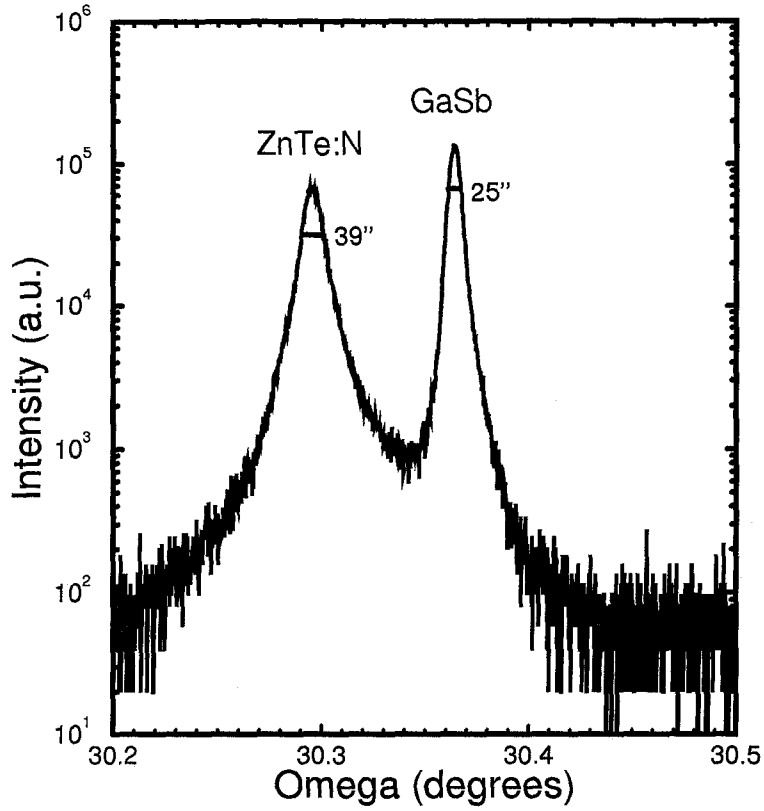

Figure 3.3: X-ray rocking curve of 1.0μm ZnTe:N epilayer doped with an RF plasma source using a dilute gas mixture of 10% N_2 / 90% Ar grown on GaSb substrate. The room temperature free hole carrier concentration is 1×10^{18}cm^{-3}. The growth prior to the II-VI layer consists of 0.6μm GaSb:Si buffer layer followed by a 20 Å AlSb blocking layer.

3.5 MBE growth of graded junction

A brief description of the technique employed to grow the graded junction region (i.e. the $Mg_xCd_{1-x}Se$ region) is presented now so as to better understand some of the complications discussed in the following chapter. A standard effusion cell loaded with elemental ingots was used for the Mg source. The Mg concentration in epilayers of $Mg_xCd_{1-x}Se$ was measured by x-ray photoemission spectroscopy (XPS). These measurements were initially checked and calibrated with electron

microprobe analysis. It was found that under identical growth conditions (substrate temperature, and source fluxes) the Mg concentration in $Mg_xCd_{1-x}Se$ was consistently reproducible. Nevertheless, prior to growing a device we would grow an epilayer of $Mg_xCd_{1-x}Se$ on a ZnTe substrate to measure the Mg concentration. This measured value was then taken to be the peak Mg concentration in the graded $Mg_xCd_{1-x}Se$ region.

3.5.1 Thermal grading of $Mg_xCd_{1-x}Se$

Presently, the graded $Mg_xCd_{1-x}Se$ region of the device is grown by simply shutting off the power to the Mg source cell, while keeping other sources static. The subsequent thermal cooling reduces the Mg flux and thus decreases the concentration in the $Mg_xCd_{1-x}Se$ region as the layer grows. The resulting grading profile is thus determined by the flux transient of the Mg. The Mg flux transient was characterized by monitoring the Mg peak in the RGA spectrum. The transient behavior was the same throughout all measurements. The CdSe growth rate was adjusted so that the whole grading would occur over $\sim 300\,\text{Å}$, and so that the Mg concentration would decrease by roughly one order of magnitude. For our particular cell and typical source material mass we noticed a consistent 1.5 minute delay after shutting off the power, before the Mg flux would begin to decrease. Once the Mg flux would start to decrease it would drop exponentially with time. Therefore, the Mg cell's power was shut off 1.5 minutes prior to the beginning of the $Mg_xCd_{1-x}Se$ graded layer. Overall, we assume that the Mg concentration in the $Mg_xCd_{1-x}Se$ layer starts at the initial measured calibration maximum, and ended up one order of magnitude lower over a total thickness of 300 Å. This technique is fundamentally limited and constrained by the thermal transient properties of the Mg source material, cell and oven. A discussion of alternative approaches will be presented in chapter 4. Despite its crude approach, this grading technique has worked sufficiently to grow graded $Mg_xCd_{1-x}Se$ layer devices capable of light

emission.

3.6 Summary

Successful p-type doping of MBE ZnTe using an RF plasma nitrogen source has enabled the use of GaSb substrates for the graded injector device discussed in the following chapter. To realize high quality ZnTe:N we employed the smallest aperture for the N-source and used a dilute 10% N_2/ 90% Ar mixture to achieve doping levels of $1\times10^{18}cm^{-3}$. Epilayer of ZnTe:N grown under these conditions exhibited room temperature PL comparable to undoped ZnTe. II-VI epitaxy on GaSb substrates is greatly improved by growing an intermediary ($\sim$ 20 Å) AlSb buffer to suppress the II-VI/III-V interfacial chemical reaction. This procedure has led to the highest quality epitaxial ZnTe:N layers grown on GaSb with x-ray FWHM of 39 arcsec. This heteroepitaxial technique and II-VI doping have been implemented to realize working graded injector LEDs.

Bibliography

[1] Y. Rajakarunanayake, B.H. Cole, J.O. McCaldin, D.H. Chow, J.R. Söderström, T.C. McGill, C.M. Jones, *Appl. Phys. Lett.* **55**, 1217 (1989).

[2] B. Voigtlander and A. Zinner, *J. Vac. Sci. Technol. A* **12**, 1932 (1994).

[3] H.J. Osten, G. Lippert and J. Klatt, *J. Vac. Sci. Technol. B* **10**, 1151 (1992).

[4] D.W. Tu and A. Kahn, *J. Vac. Sci. Technol. A* **3**, 922 (1985).

[5] D.R. Menke, J. Qiu and R.L. Gunshor, *J. Vac. Sci. Technol. B* **9**, 2171 (1991).

[6] W.G. Wilke and K.Horn, *J. Vac. Sci. Technol. B* **6**, 1211 (1988).

[7] M.P. Halsall, D. Wolverson, J.J. Davies, B. Lunn and D.E. Ashenford, *Appl. Phys. Lett.* **60**, 2129 (1992).

[8] C.T. Chou, J.L. Hutchison, D.Cherns, M.J. Casanove, J.W. Steeds, R. Vincent, B. Lunn and D.A. Ashenford, *J. Appl. Phys.* **74**, 6566 (1993).

[9] N.J. Duddles, J.E. Nicholls, T.J. Gregory, W.E. Hagston, B. Lunn and D.A. Ashenford, *J. Vac. Sci. Technol. B* **10**, 912 (1992).

[10] J. Petruzzello, B. Greenberg and J. Gaines, *Bull. Am. Phys. Soc.* **35**, 237 (1990).

[11] Eagle-Picher Research Laboratory, Miami, Oklahoma.

[12] R. Miles, J. Swenberg, M. Wang, M. Phillips and T. McGill, *J. Cryst. Growth* **138**, 523, (1994).

[13] E. Yu, M. Phillips, D. Chow, D. Collins, M. Wang, J. McCaldin and T. McGill, *Phys. Rev. B* **46**, 13379 (1992).

[14] R. Feldman, R. Austin, A. Sher, M. Schnoes, S. Downey, A. Emerson, T. Harris, R. Spitzer, G. Gualtieri and G. Schwartz, *J. Cryst. Growth* **118**, 295 (1992).

[15] Y. Hishida, H. Ishii, T. Toda and T. Niina, *J. Cryst. Growth* **95**, 517, (1989).

[16] F. Turco-Sandroff, M. Brasil, R. Nahory, R. Martin, Y. Zhang and B. Skromme, *Appl. Phys. Lett.* **59**, 688, (1991).

[17] K. Ohkawa, T. Karasawa and T. Mitsuyu, *J. Cryst. Growth* **111**, 797, (1991).

[18] R. Park, M. Troffer, E. Yablonovitch and T. Gmitter, *Appl. Phys. Lett.* **59**, 1896, (1991).

[19] J. Qiu, H. Cheng, J. Depuydt and M. Haase, *J. Cryst. Growth* **127**, 279, (1993).

[20] J. Petruzzello, J. Gaines, P. van der Sluis, D. Olego and C. Ponzoni, *Appl. Phys. Lett.* **62**, 1496, (1993).

[21] Oxford Applied Research, Crawley Mill, Witney, Oxfordshire OX8 5TJ, UK

[22] T. Ohtsuka and K. Horie,*Jpn. J. Appl. Phys.* **32**, L233, (1993).

[23] R. Vaudo, J. Cook and J. Schetzina, *J. Cryst. Growth* **138**, 430, (1994).

[24] J. Han, T. Stravrinides, M. Kobayashi, R. Gunshor, M. Hagerott and A. Nurmikko, *Appl. Phys. Lett.* **62**, 840, (1993).

[25] J. Swenberg, M. Wang, R. Miles, M. Phillips, A. Hunter, J. McCaldin and T. McGill, *J. Cryst. Growth* **138**, 692, (1994).

[26] I. Tao, M. Jurkovic and W. Wang, *Appl. Phys. Lett.* **64**, 1848, (1994).

[27] Y. Fan, J. Han, L. He, J. Saraie, R. Gunshor, M. Hagerott, H. Jeon, A. Nurmikko, G. Hua and N. Otsuka, *Appl. Phys. Lett.* **61**, 3160, (1992).

[28] Specification sheet for Model MPD21 Atom/Radical Beam Source, Oxford Applied Research, Crawley Mill, Witney, Oxfordshire OX8 5TJ, UK

[29] Temperature Hall measurements were performed by Dr. A.T. Hunter of Hughes Research Laboratories, Malibu, California 90265. Room temperature and liquid nitrogen temperature measurements were performed at Caltech by author.

[30] Z. Zhu,H. Mori and T. Yao, *Appl. Phys. Lett.* **61**, 2811, (1992).

[31] Gerald Burns, *Solid State Physics* (Academic Press, Inc., 1985), pp. 163.

[32] PC-HRS Version 1.0, High resolution simulation program for PC, Dr. P. Fewster, Philips Research Laboratories, Redhill U.K.

Chapter 4

Development of the Graded Injector Light Emitter

4.1 Introduction and outline

The early graded injector devices were severely limited by the lack of a MBE p-type dopant for ZnTe, a high quality substrate, and the lack of sufficient materials characterization of $Mg_xCd_{1-x}Se$ necessary for a realistic approach to device engineering. In spite of these shortcomings, the early devices fabricated using ZnTe substrates appeared to work as LEDs but only under high biases and a restrictive device design [1].

In this chapter, we report on advances in the development of the graded junction electron injector device, i.e. the graded injector. Materials characterizations of the $Mg_xCd_{1-x}Se$ alloy necessary for device engineering issues are presented. Success in p-type doping of ZnTe, discussed in the previous chapter, has subsequently enabled the use of higher quality GaSb substrates. Devices grown with GaSb substrates show the benefits of high quality substrates. Present electrical characteristics exhibiting normal diode-like behavior more clearly demonstrate the operating principle of the graded injector over the previous studies of Phillips *et*

al. [2]. Electroluminescence (EL) characteristics of the graded injector LED are presented along with a discussion of the the optical performance. These results lay the foundation for and highlight the salient issues for further studies needed to advance the graded injector device development to a point of commercial interest.

4.2 Device engineering

There have been very few studies of the epitaxial growth of Mg chalcogenides. Early studies of Itoh [3] synthesized *p-n* diodes based on $Mg_xCd_{1-x}Te$ crystals grown by the Bridgman-Stockbarger method. Okuyama *et al.* [4] grew and characterized epilayers of $Zn_xMg_{1-x}S_ySe_{1-y}$ and proposed and subsequently demonstrated [5] the use of this quaternary as lattice matched cladding layers in blue-green laser diodes. More recently, MgTe and $Mg_xCd_{1-x}Te$ thin films grown by MBE have been reported [6]. But there have been no reported studies of $Mg_xCd_{1-x}Se$ alloy epilayers. The original design of the graded $Mg_xCd_{1-x}Se$ region was made based on approximations of the material parameters due to this lack of characterization.

For efficient operation of the graded injector, the conduction band must be properly graded to avoid any energy barrier to electrons at the Se/Te interface. Ideally we would want to continuously grade the conduction band from that of ZnTe down to CdSe. Device simulations suggest that small discontinuities in the conduction band may be acceptable for device operation, but we would like to reduce and eliminate any electron barrier at the $Mg_xCd_{1-x}Se$/ZnTe interface. In fact it would be prefered that the conduction band of $Mg_xCd_{1-x}Se$ be graded above that of ZnTe rather than below. This has the unfortunate consequence of introducing more strain due to the higher Mg concentration. So we would like to be as close as possible to a continuous grading at the $Mg_xCd_{1-x}Se$/ZnTe interface. To accomplish this, it is necessary that we know the position of the band edges of $Mg_xCd_{1-x}Se$ as a function of Mg concentration. To do this, we

need the band gap as a function of Mg concentration and the relative valence band offset. The estimates of the band gap of MgSe range from 3.6 to 5.6 eV [4, 7]. Therefore we need an accurate measure of the $Mg_xCd_{1-x}Se$ band gap as a function of Mg concentration. Furthermore, there had been no previous studies of the valence band offsets for the Mg chalcogenides, and we would expect a deviation from the common anion rule similar to that observed in the AlAs/GaAs system, since Mg like Al has unoccupied *d* orbitals [8, 9]. Therefore it becomes critical to experimentally measure the valence band offset of the $Mg_xCd_{1-x}Se/CdSe$ system.

4.2.1 Band gap studies of $Mg_xCd_{1-x}Se$

Pseudomorphic epilayers of cubic $Mg_xCd_{1-x}Se$, with x ranging from 0 to 63%, were grown on (100) ZnTe substrates with thicknesses of at least 1000 Å. The Mg concentration was reproducibly grown and measured by XPS, after calibrating with electron microprobe analysis. The RHEED pattern during the $Mg_xCd_{1-x}Se$ growth exhibited a Se-rich (2 × 1) streaky reconstructed surface. The RHEED pattern showed no indications of any deviation from cubic material even for layers grown slightly beyond the critical thickness. X-ray diffraction patterns of $Mg_xCd_{1-x}Se$ epilayers also indicated a cubic crystalline structure, although with large FWHMs and a high degree of crystalline mosaicity.

A characteristic photoluminescence (PL) spectra from a $Mg_xCd_{1-x}Se$ epilayer is represented in Figure 4.1. A He-Cd laser (325nm) with 1mW power was used for the excitation source. The broad high energy peak is thought to be a donor-to-acceptor pair (DAP) emission from the $Mg_{.46}Cd_{.56}Se$ epilayer. Since the epilayer is grown beyond the critical thickness and has poor structural quality, there is no excitonic emission. Additionally, there is increased deep emission associated with the $Mg_{.46}Cd_{.56}Se$ layer.

The band gap energy of the epilayers was estimated from the high energy peak band edge emission in the PL spectrum at 5K. We could not use the room temper-

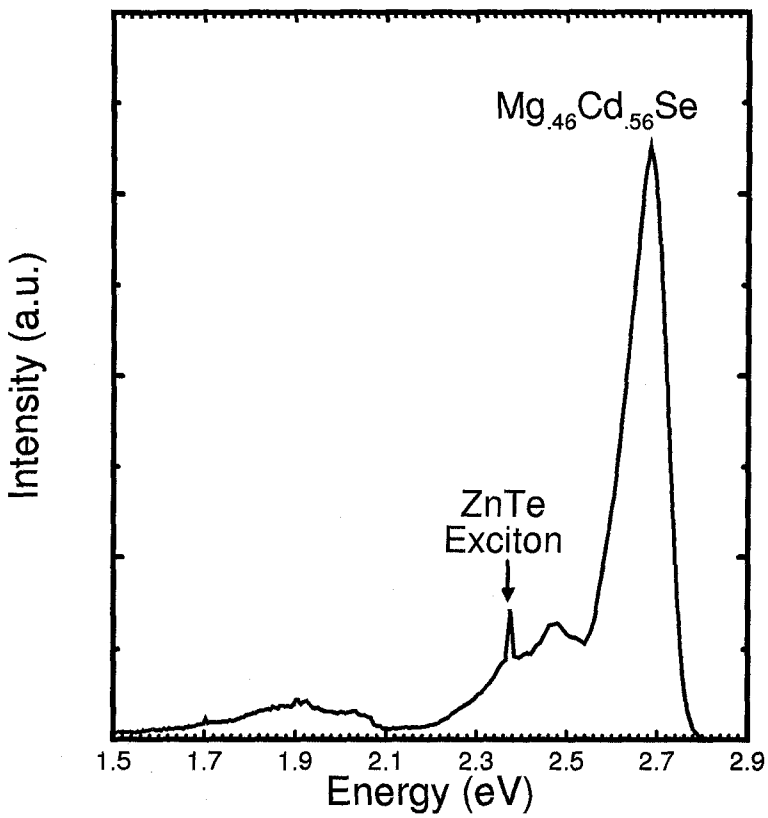

Figure 4.1: Low temperature (5K) photoluminescence (PL) spectra of 1000 Å $Mg_{.46}Cd_{.56}Se$ epilayer grown on ZnTe substrate. 1mW excitation from HeCd (325nm) laser. An excitonic peak from the underlying ZnTe is indicated. The high energy broad peak is from the $Mg_{.46}Cd_{.56}Se$ layer. This peak is thought to be a donor-to-acceptor pair (DAP) emission. No excitonic emission is observed from the $Mg_{.46}Cd_{.56}Se$ epilayer due to the poor structural quality of the layer grown past the critical thickness. This may also be responsible for the deep emission which would be reduced under more optimal growth conditions.

ature PL spectra due to severely degraded emission for the high Mg concentration layers. The DAP emission is a lower bound for the band gap at 5K. We expect the band gap to be greater than 100 meV above the DAP emission based on the deep acceptor states of the wide band gap II-VIs associated with the heavy hole mass in the valence band. At room temperature, the band gap would be from 100-140 meV less than the 5K band gap, which is typical of the II-VIs. So we can conservatively regard the band edge emission as the band gap for these alloys. For the low concentration Mg layers this estimate was found to be consistent. The band gap energy as a function of Mg concentration is plotted in Figure 4.2. We notice a deviation from a linear dependence on Mg concentration. Fitting the data to a quadratic function we extrapolate a band gap for MgSe to be 4.54 eV. The specific band gap of MgSe is not necessarily important, but what is relevant is the position of the $Mg_xCd_{1-x}Se$ conduction band relative to that of CdSe and ZnTe as a function of Mg concentration. To do determine this we need a measure of the valence band offset of $Mg_xCd_{1-x}Se$.

4.2.2 Valence band offset measurement of $MgSe/Cd_{.56}Zn_{.44}Se$

The valence band offset (VBO), ΔE_v, of $MgSe/Cd_{.56}Zn_{.44}Se$ was measured by Wang *et al.* [10] using X-ray photoelectron spectroscopy (XPS). This heterojunction is used so as to avoid difficulties associated with lattice strain. Bulk MgSe naturally occurs in the NaCl structure, but the zinc blende lattice constant has been extrapolated by Okuyama *et al.* [4] to be about 5.89 Å. The lattice matched $Cd_{.56}Zn_{.44}Se$ alloy composition was measured and calibrated using X-ray diffraction for lattice constant and XPS for alloy concentration. We used (100) GaSb substrates with GaSb buffer layers to provide a high quality smooth growth surface. A thick buffer layer of ZnTe was grown on the GaSb substrates since this II-VI/III-V heteroepitaxial growth technology was well advanced. Next, thick relaxed layer of $Cd_{.56}Zn_{.44}Se$ with a lattice constant of 5.93 Å provide closely lattice

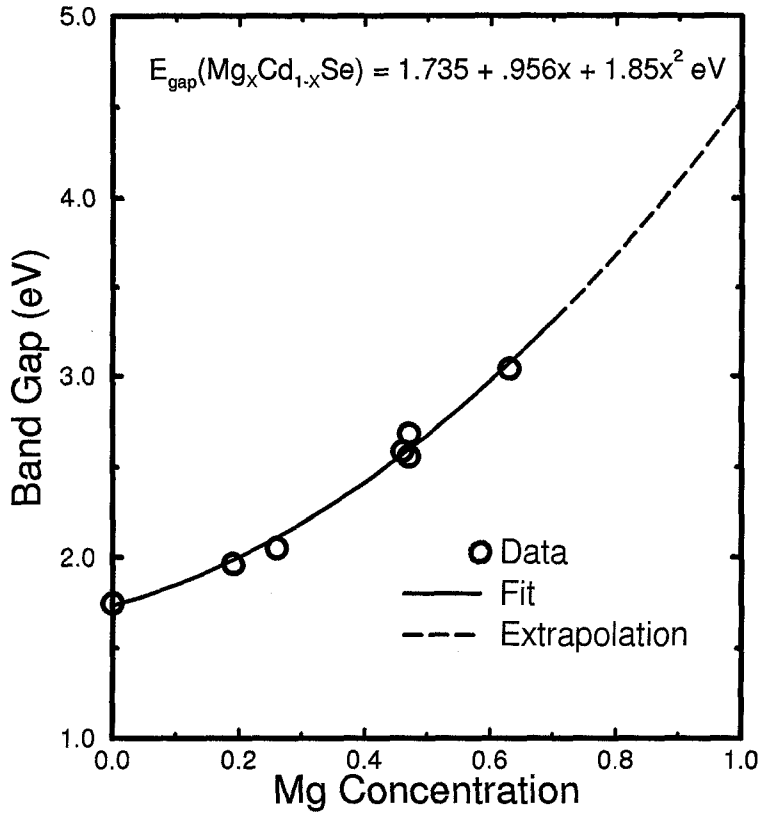

Figure 4.2: Estimated band gap of $Mg_xCd_{1-x}Se$ alloy as a function of Mg concentration. Data taken from low temperature PL spectra is used to approximate the room temperature band gap. Experimental data is best fit by a quadratic equation. Extrapolation of the fit estimates the band gap of zinc blende MgSe to be 4.54 eV.

matched layers for the XPS experiment. The MgSe epilayers were grown up to a maximum of about 150 Å. During growth these layers exhibited a streaky (2 × 1) RHEED diffraction pattern indicating zinc blende epitaxial growth.

The value obtained for the VBO is [10]:

$$\Delta E_v\ (MgSe/Cd_{.56}Zn_{.44}Se) = 0.56 \pm 0.07eV. \tag{4.1}$$

4.2.3 Band edge engineering

We can construct the band edge (BE) positions, valence band edge (VBE) and conduction band edge (CBE), relative to the BE's of CdSe and ZnTe for the $Mg_xCd_{1-x}Se$ alloy as a function of Mg concentration. Using the above measured value for the $MgSe/Cd_{.56}Zn_{.44}Se$ VBO and CdSe/ZnTe VBO of 0.64 eV [11] we plot the position of the valence band of $Mg_xCd_{1-x}Se$ relative to the VBEs of CdSe and ZnTe. Here we assume no band bowing and a linear dependence in the VBE going from CdSe to MgSe. Adding to this the band gap information for $Mg_xCd_{1-x}Se$, we plot the CBE of $Mg_xCd_{1-x}Se$ relative to the CBE of ZnTe. From this plot we extract an approximation for the $Mg_xCd_{1-x}Se$ alloy which will have its CBE aligned with the CBE of ZnTe. We estimate this is accomplished with a Mg concentration of 69 %. Therefore, for the graded device we use this estimate for the initial Mg concentration in the $Mg_xCd_{1-x}Se$ alloy junction.

4.3 Device structure

Light emitting devices based on the graded injector design have been grown on both (100) GaSb substrates and (100) p-ZnTe substrates. Devices grown on GaSb showed significantly better structural, electrical and optical properties than those grown on the ZnTe, so we concentrated on those with GaSb substrates. The poor performance of the ZnTe substrates appeared to be due to the presence of Te precipates in the substrates as well as the formation of dislocations due to poor surface quality. Log plots of the J-V characteristics of devices on ZnTe substrates showed large leakage currents and reduced optical performance resulting from the structural defects. Ideally, we would prefer ZnTe substrates rather than GaSb, but lacking a suitable commercial source for ZnTe the best available choice was GaSb.

A typical device structure is grown on a GaSb substrate indium bonded for thermal conduction to a molybdenum block. In the III-V MBE chamber a 3000 Å

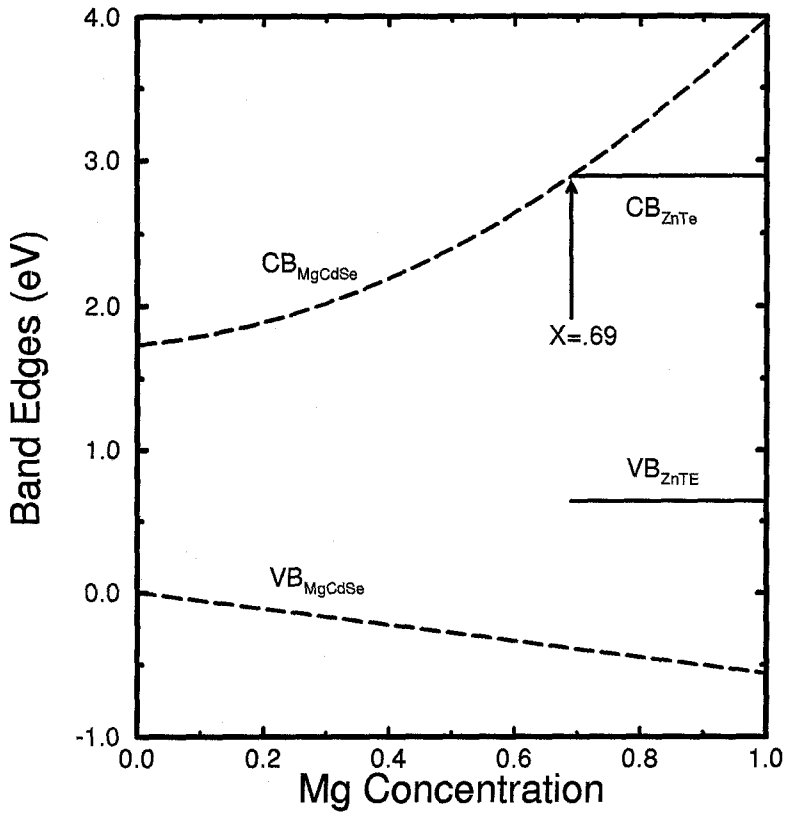

Figure 4.3: Band edge alignment of $Mg_xCd_{1-x}Se$ alloy as a function of Mg concentration. Conduction (CBE) and valence band edge (VBE) positions are relative to the VBE of CdSe. Using the band offsets of CdSe/ZnTe and $MgSe/Cd_{.56}Zn_{.44}Se$ and assuming a linear variation in the VBE of $Mg_xCd_{1-x}Se$ together with the band gap dependence of $Mg_xCd_{1-x}Se$ we construct the band edge dependence. With these assumptions we estimate a 69% concentration of Mg in $Mg_xCd_{1-x}Se$ is needed to align the conduction bands of $Mg_xCd_{1-x}Se$ and ZnTe.

GaSb:Si buffer layer followed by a 20 Å AlSb cap is grown. The sample is transferred via UHV to the II-VI chamber, where growth of the device proceeds at a growth temperature of 300 °C. The device consists of $\sim$ 1 μm of ZnTe:N doped to roughly 1×10^{18}cm^{-3} hole carrier concentration. Next the graded $Mg_xCd_{1-x}Se$ layer with thickness varying from 300-600 Å is grown . $Mg_xCd_{1-x}Se$ layers with maximum concentrations from 60-70% Mg at the ZnTe interface were graded down to about one order of magnitude less Mg $\sim$ 6-7 %. The final n-junction layer consists of $\sim$ 300 Å CdSe:Al doped to about 1×10^{19}cm^{-3}.

4.3.1 Device fabrication

Device fabrication relies on standard lithographic and wet etch techniques. After pulling the samples from UHV, we heat the moly block in an inert atmosphere glove box to remove the substrate's indium bonding. We use a controlled environment to avoid any potential oxidation. The diodes are then lithographically defined into octagon mesas with areas of 1.8×10^{-4} cm^2. Electrical isolation is formed with a 0.5% bromine:ethylene-glycol wet etch 4000 Å into the p-ZnTe layer, well beyond the p-n junction. Lateral ohmic contacts to the p-ZnTe and top contacts to the CdSe:Al are made with evaporated Au/Ge and defined by standard photolithographic lift-off procedures. An ohmic back contact to the GaSb substrate can also be used but there is a 0.82 eV valence band offset for GaSb/ZnTe which lead to resistance across this interface. This effect is slightly mitigated due to the large area of the interface and the high doping concentrations but it still makes the back contact through the GaSb more resistive than the front lateral contacts. The devices are then placed on a TO-5 header, wire bonded and available for electrical and optical characterization.

4.4 Material characterization

4.4.1 TEM

Transmission electron microscopy (TEM) studies [12] of the junction region of the devices revealed a number of interesting features. We discovered that the actual thickness of the $Mg_xCd_{1-x}Se$ region in devices grown were significantly thicker than expected. As previously described in chapter 3, we adjusted the growth of the $Mg_xCd_{1-x}Se$ by calibrating the growth of CdSe to the thermal transient of the Mg flux. The growth of the alloy appears to be significantly faster than anticipated given the growth rate of CdSe and the additional Mg. We expected only 300 Åfor the graded region but were actually growing almost twice as thick. The presence of Mg, with a sticking coefficient of 1, seems to increase the sticking coefficient of Cd thereby increasing the overall growth rate.

We believe a thinner grading is essential but will be very sensitive to the growth technique used. This is apparent in the TEM images of the $Mg_xCd_{1-x}Se$/ZnTe interface. This interface is characterized by the appearance of an interfacial reaction and point defect formation leading to stacking faults in the [111] direction. We estimate well over 1×10^{10} cm^{-2} defect densities in the graded regions.

Due to the fixed constraints of this method of grading the $Mg_xCd_{1-x}Se$ region, we have been unsuccessful in fully compensating for this growth anomaly. Attemps to shutter the Mg cell or slow down the overall growth rate helped to reduce the graded region thickness but to the detriment of device performance compared to the devices with thicker grading. The reason for this phenomena still needs to be addressed.

We believe that by properly controlling the Mg source we can both decrease the grading thickness and reduce defect formations. We have investigated the use of two potential alternative source cells to better control the flux. One likely candidate is a valved cell, where a mechanical valve can adjust the beam flux

precisely without changes in source temperature. The other is a water cooled Knudsen cell, where the thermal transients are reduced with very efficient cooling. Both cells would allow for extremely quick flux decreases necessary for a thinner grading. Ideally though, the valved cell is prefered because of its ability to variably control fluxes independent of thermal transients. A full range of valve positions from open to completely closed can be reached in seconds. Therefore, a grading with precise Mg concentration can be achieved in well under 300 Å. Unfortunately, this type of cell has not yet been used with Mg as the source material and issues of reliability and materials compatibility have not yet been determined.

4.4.2 X-ray

Figure 4.4 shows the X-ray rocking curve data from the (004) reflection of a graded device structure grown on a GaSb substrate. Included in the plot is a computer simulated rocking curve generating using the PC-HRS software of Fewster [13]. The FWHM of the GaSb and ZnTe layers are 25 and 39 arc seconds respectively. The ZnTe epilayer of this device is coherently strained to the GaSb substrate. This is confirmed by analyzing the asymetric (115) diffraction peaks relative to the GaSb peak. The CdSe layer has a broad FWHM and weak amplitude close to the theoretically expected values given the finite thickness ($\sim$ 300 Å) of the layer. Most striking is the presence of the zinc blende diffraction peak of the CdSe. This confirms the growth of cubic material through the graded $Mg_xCd_{1-x}Se$ region.

Surprisingly, it was noticed that the structural quality of the device epilayers,as measured by the ZnTe FWHM, was not correlated with the electrical and/or optical performance of the LED. In fact, the best performing device with the highest external quantum efficiency had a much worse ZnTe FWHM than the device in Figure 4.4. These results imply that it is not the structural quality of the ZnTe material that is presently limiting the LED performance. The luminescence quality of all the epilayers (excluding the fully relaxed thick layers) appear to be equiv-

alent as measured by PL intensities. Therefore it appears that the devices are limited by the injection efficiency rather than the recombination efficiency. The injection efficiency is primarily dependent on the $Mg_xCd_{1-x}Se$ graded region and $Mg_xCd_{1-x}Se$/ZnTe interface. This issue of device efficiency will be discussed later in the chapter.

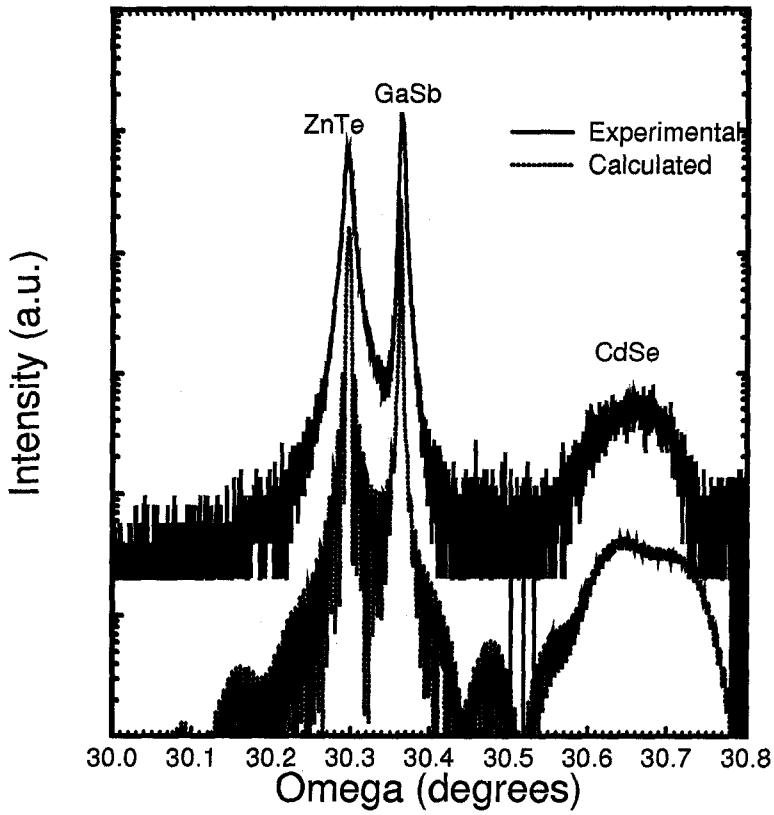

Figure 4.4: The (004) reflection X-ray rocking curve of a graded device grown on a GaSb substrate. Included is a calculated rocking curve for the same device structure. The simulated curve is generated using the PC-HRS software from Philips Research Laboratories. We notice the zinc blende (004) peak of the CdSe layer indicating cubic growth through the grading. The slight shoulder on the high angle side of the simulated curve of the CdSe peak originates from the $Mg_xCd_{1-x}Se$ grading. Data was aquired using a four-crystal Ge-monochrometer diffractometer.

4.5 Device operation

4.5.1 Electrical performance

Figure 4.5 shows a comparison of the room temperature electrical characteristics of the original and the present graded devices. The original device's electrical properties shortcomings have been eliminated by being able to grow doped layers of p-ZnTe. The high series resistance of the early devices was due to the low conductivity of the ZnTe substrates, and the high turn-on voltage was probably due to the charging of traps at or near the substrate/buffer layer interface and the thin undoped ZnTe epilayer all together resulting in a large voltage drop across this region. The present devices' current-voltage characteristics are very good. These devices turn on more like an ordinary diode and operate at a voltage near the band gap of ZnTe. There is almost no reverse bias leakage current and a sharp forward bias turn-on. Most of the series resistance in the present device (25 Ω) comes from current spreading through the thin ZnTe:N epilayer and not from the contact or junction region. This has been substantiated by the linear dependence of the resistance through the p-ZnTe epilayer as a function of contact to contact seperation. This small series resistance can be virtually eliminated with the use of high quality p-ZnTe substrates and/or thicker epilayers of p-ZnTe on GaSb.

To better understand the current injection mechanisms in the LED, we plot the current density on a log scale as seen in Figure 4.6. Plotted in this manner we can extract the ideality factor (n) for a diode. n is used and given by a modification to the basic diode current-voltage equation to account for space-charge recombination current. A simple empirical representation of the current-voltage relation is thus given by the following formula:

$$I_{Diode} \sim e^{qV/nkT}. \tag{4.2}$$

An ideality n=1 would be the case for a pure diffusion current, while an ideal-

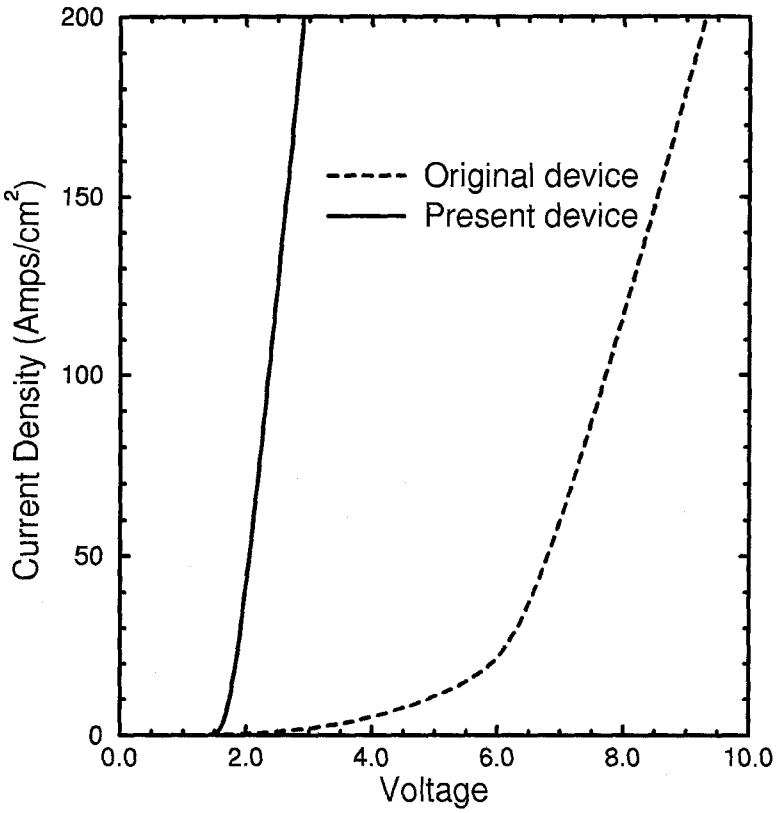

Figure 4.5: Room temperature electrical characteristics of the original and present graded devices. The original device is a 100 μm diameter mesa with back contacts made to the ZnTe substrate. The present device grown on GaSb is an octagon mesa with an area of 1.8×10^{-4} cm^2 with front lateral contacts made to the p-ZnTe epilayer.

ity n=2 would be for pure recombination current based on the Shockley-Read-Hall model of recombination through a trap [17]. When both currents are comparable, the ideality will vary between 1 and 2. A more accurate current-voltage relation would equate the total diode current to the sum of a diffusion current plus various space-charge (non-radiative) recombination currents. This would account for deviations from pure diffusion current, but would be an intractable J-V relation. Nevertheless, the simple model using an ideality factor gives insight into the processes associated with the diode current mechanisms.

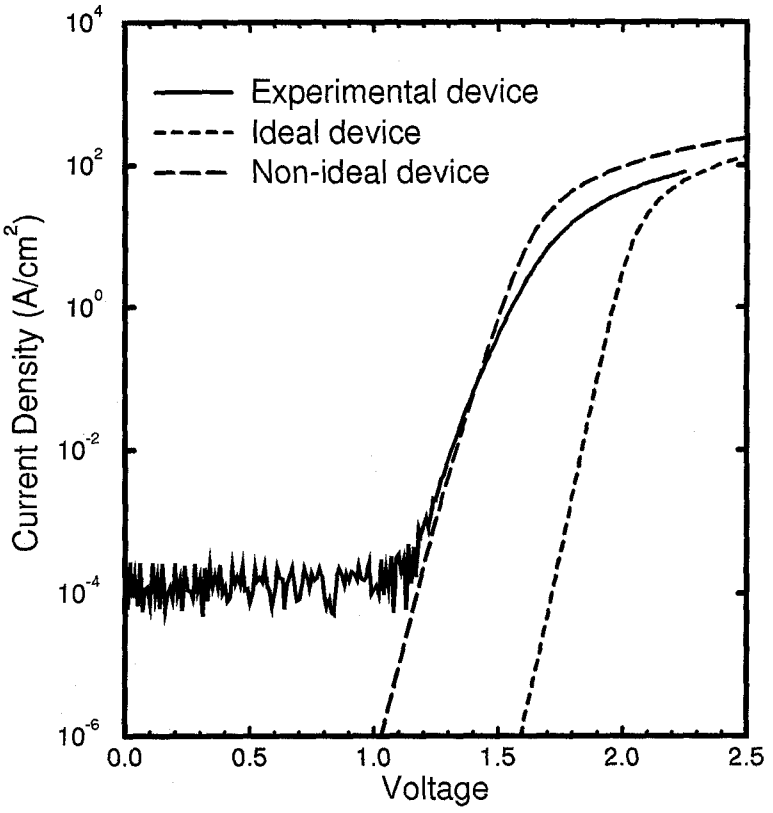

Figure 4.6: Log plots of current density vs. voltage for an experimental device, and simulated "ideal" and "non-ideal" graded devices. The ideal device has a continuous grading in the conduction band and negligible space-charge recombination at the $Mg_xCd_{1-x}Se/ZnTe$ interface. By construction the ideality of this ideal device is n=1, which indicates pure diffusion current. The non-ideal device has a 300 meV discontinuity at the $Mg_xCd_{1-x}Se/ZnTe$ interface and a significant density of interface traps. The minimum ideality of the experimental device is n=1.8 indicating a combination of diffusion and space-charge recombination currents.

The minimum ideality for the experimental data is n=1.8. This indicates a combination of diffusion and interfacial-recombination currents. With higher injection currents, the series resistance distorts the ideality factor making it appear larger. Plotted along with the experimental data are simulated results using the model of Wang *et al.* [18] based on the drift-diffusion transport equations. The computer model used to generate the J-V behavior of the device can be used to intuitively explain the non-ideal behavior of the experimental device.

The "ideal" case corresponds to a graded device with a continuous conduction band and a negligible number of non-radiative recombination centers at the $Mg_xCd_{1-x}Se$/ZnTe interface. The effective surface recombination velocity at this interface was assumed to be 200 cm/sec. Not surprisingly, the ideality for this case is n=1. We can modify the qualitative and quantitative behavior of the J-V by adjusting the interface trap concentration and the grading discontinuity. As the density of traps at the $Mg_xCd_{1-x}Se$/ZnTe interface is increased the non-radiative space-charge current will increase. A discontinous grading in the conduction band resulting in an electron barrier at the $Mg_xCd_{1-x}Se$/ZnTe interface leads to an accumulation of electrons at this interface and subsequently enhances any non- radiative recombination processes. Increased space-charge current will both increase the ideality and shift the log J-V curve upwards towards the experimental curve.

As an example, we plot in Figure 4.6 the simulation result for a "non-ideal" device. This device had a discontinuous grading, with a 300 meV discontinuity at the $Mg_xCd_{1-x}Se$/ZnTe interface, and a high density of interface traps with an effective surface recombination velocity of 1×10^9 cm/sec. The actual value of the discontinuity isn't the important parameter in this calculation. Physically what matters is the presence of non-radiative channels at the interface, and an overlap of carrier accumulation at this interface. We should not take the parameters as physically meaningful but as illustrative of the trend and behavior of the interface properties. From this behavior we conclude the interfacial non-radiative current is non-negligible in our present graded devices. Furthermore, it is most likely the

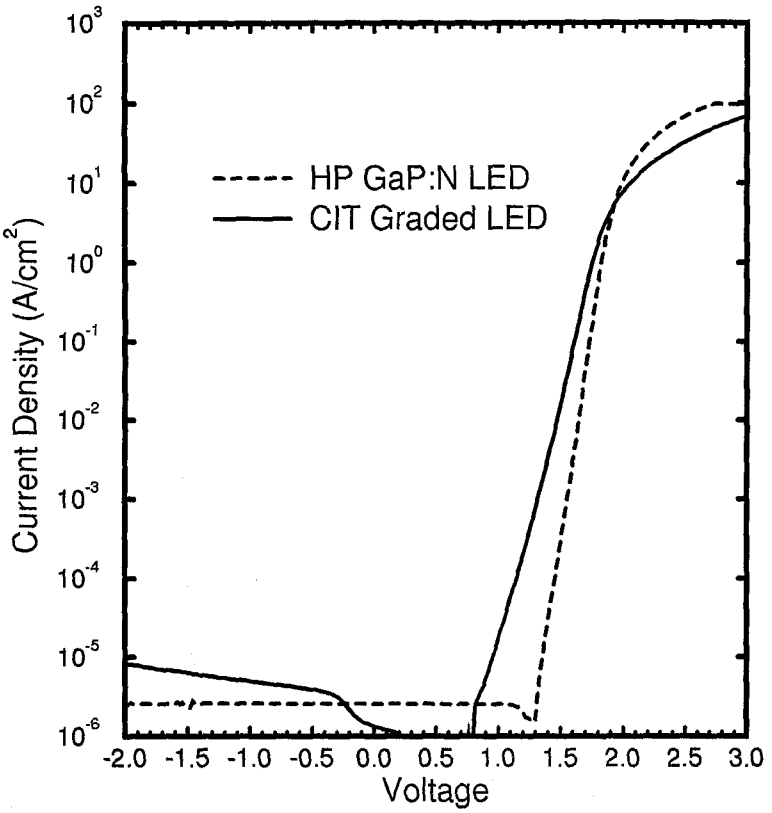

Figure 4.7: Log plot of graded injector LED compared to Hewlett Packard commercial GaP:N green LED. Both devices exhibit small reverse bias saturation currents and obvious indications of the onset of forward bias current injection. The GaP:N LED begins to emit light at 1.75 Volts forward bias and the Caltech graded LED begin at 1.85 Volts.

grading in the device is not optimized and there exists an electron barrier at the interface. In spite of the interfacial problems the device operates as a normal LED as will be discussed later.

In Figure 4.7 a log plot of the room temperature J-V characteristics of a graded device is compared with a commercial GaP:N green LED. Both devices show similar J-V behavior, with the graded device having slightly more space-charge recombination current and larger series resistance. Light emission turn-on, as defined by when you can begin to see light with the eye, is coincidentally very similar in

the two devices as well. The commercial device begins to turn-on at about 1.75 Volts, and the graded device begins to turn-on at about 1.85 Volts. Light emission can begin at voltages below the band gap due to the minority carrier injection process [19]. Although the graded junction LED has a drastically different device design and operating concept compared to the standard commercial LEDs, we see remarkably similar operating characteristics.

4.5.2 Optical performance

Electroluminescence

Figure 4.8 shows a characteristic electroluminescence (EL) spectra from a graded device operating under a 2.8 Volts DC bias at room temperature. The EL spectra clearly demonstrates the electron injection into the p-ZnTe. The emission is dominated by band to band recombination in the ZnTe at 2.25 eV, with no deep emission present. The absence of any luminescence from CdSe ($E_{gap} = 1.74$ eV) indicates that holes are blocked by the valence band offset barrier. The lower energy emission centered at 1.96 eV is currently not conclusively known. This red emission peak is present in all graded devices fabricated to date. The relative intensity of this peak compared to the band edge emission varies from sample to sample and appears to be independent of substrate (ZnTe or GaSb) and growth conditions. This 1.96 eV red peak is not present in the photoluminescence of ZnTe:N epilayers. Although, it is observed in the photoluminescence of graded device structures as well as epilayers of CdSe:Al on ZnTe:N (the same structure of a graded device without the $Mg_xCd_{1-x}Se$ layer). In the case of the CdSe:Al/ZnTe:N structure the luminescence of the red peak is weaker than for the comparable graded device structure. Therefore, we believe the red luminescence to be related to the Se/Te interface, and the magnitude of its effect is increased with the presence of Mg. The exact nature of this phenomena is still under investigation.

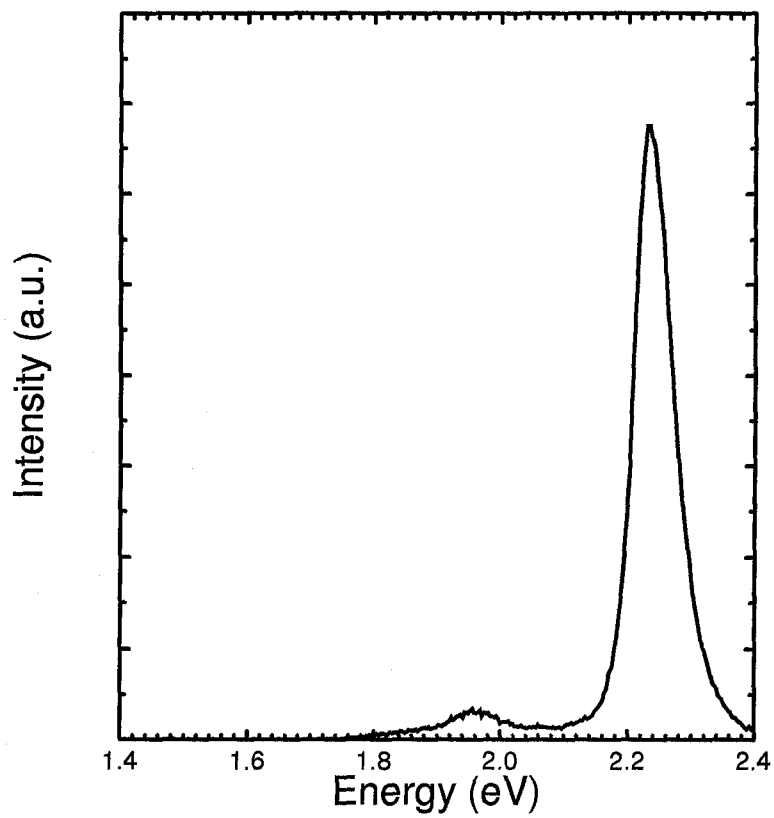

Figure 4.8: Room temperature electroluminescence spectra of a graded injector device. Device is a hexagon mesa with an area of 1.8×10^{-4} cm^2 operating under a 2.8 Volt DC bias with 30mA current. Emission is dominated by band to band recombination of ZnTe. No luminescence is observed from CdSe or from deep emission. The low energy emission at 1.96 eV is believed to be from the Se/Te interface.

Quantum efficiency

The external quantum efficiency η_{ext}, defined as the ratio of the number of photons emitted from a device to the number of charge carriers passing through the diode, was measured using an "Integrating Sphere" [20]. A Si photodetector is fit to the sphere to detect the radiant flux. Geometric and reflectivity effects of the sphere were calibrated using commercial LEDs with known quantum efficiencies. The best measured external quantum efficiency of the graded injector LED grown on GaSb substrates was 0.007%. This is close to an order of magnitude greater than the best of the early devices grown on ZnTe substrates. In spite of the improvement in performance, the present graded devices in there current state are not competitive with commercial green LEDs, although we have made little effort in optimizing light extraction which could drastically improve overall η_{ext}. We have focused instead on developing the technology to clearly demonstrate graded injection in an LED.

To examine the reasons for the devices' lower efficiencies and offer suggestions for improvements we break the external quantum efficiency into three independent terms, each which comprises a separate physical component for the overall efficiency. These elements of the external quantum efficiency η_{ext} are,

$$\eta_{ext} = \eta_i \cdot \eta_r \cdot \eta_x \tag{4.3}$$

where η_i is the injection efficiency, η_r is the recombination efficiency, and η_x is the light extraction efficiency.

Since the luminescence is generated in the p-region, the injection efficiency, η_i, is the ratio of the electron injection current to the total current. The total current is composed of the electron injection, hole injection and space-charge recombination. We saw previously there is negligible hole current, but significant interfacial recombination current. To improve the injection efficiency we must reduce the space-charge recombination current. To do this will require better control and understanding of the $Mg_xCd_{1-x}Se$/ZnTe interface and graded $Mg_xCd_{1-x}Se$ region.

The recombination efficiency, η_r, is the ratio of the radiative recombination to the total recombination in the p-region of the device. Here there are a few factors which limit the efficiency. The thickness and quality of the ZnTe active region will strongly effect the recombination efficiency. In our device structure, if the electron diffusion length is comparable to the thickness of the ZnTe ($\sim 1\mu$m) then η_r would be reduced by the carriers recombining in the GaSb. Mathine *et al.* [21] found for thick (up to 2μm, which is far greater than the absorption length of the laser excitation, 4400 Å) ZnTe epilayers grown on GaSb buffer layers an appreciable PL recombination from the underlying GaSb, indicating the diffusion of carriers through the ZnTe. Attempts at growing thicker ZnTe epilayers are limited by the critical thickness of these epilayers grown on GaSb. On the other hand the luminescent quality of the ZnTe material is very good, as seen in the room temperature PL and the absence of deep emission. One way to mitigate the thickness limitations and improve the recombination efficiency is to incorporate quantum wells and quantum well structures to capture carriers and provide higher radiative recombination efficiencies. We estimate that quantum well structures could improve radiative efficiencies by at least one order of magnitude. Epilayers of ZnTe with $Cd_xZn_{1-x}Te$ quantum wells have been seen to improve the integrated PL by over an order of magnitude as compared to ZnTe epilayers with no quantum wells. Working graded injectors with quantum wells have not to date been grown but are currently being investigated.

The extraction efficiency, η_x, is the ratio of the number of photons which escape the LED to the total number generated in the active region. This factor is pricipally governed by the device design and fabrication, *i.e.* the presence of absorbing materials, the type and position of contacts, the fabrication of cubes rather than mesas, and encapsulation techniques. The extraction of light is fundamentally limited by the critical angle for total internal reflection (Snell's Law), and absorbtion. The extraction of light generated by an LED has in fact been a major focus of commercial interest [22, 23, 24]. By using thick transparent conducting window layers

to allow for current spreading and moving the junction away from the top contact, Huang *et al.* [22] increased external quantum efficiencies by a factor of twofold. Kish *et al.* [23] used a wafer-bonding technique to replace an absorbing substrate with a transparent substrate to increase the external efficiency by a factor of 2 as well. Encapsulation and packaging are standardly used in commercial LEDs to increase extraction by up to a factor of 8 [24]. Since we are using absorbing GaSb substrates, all the light emitted down into the device is lost. Furthermore, since the p-n junction is just below the top contact (< 1000 Å) there is little current spreading and all the light generation is underneath the contact. The top contact, Au/Ge, is not transparent and prevents any extraction through the top of the device. In our devices the observed light escapes only from the perimeter of the contact and edges of the mesa. As a result the extraction efficiency is extremely poor. We have made no serious effort to improve the extraction efficiency although Wang [25] has suggested some possible top contacting schemes to improve the light extraction. In addition if ZnTe substrates were available we would then have transparent substrates. Bulk growth of ZnTe substrates has not been very advanced. One way to overcome this problem, would be to use thick layers ($>$ 100 μm) of ZnTe grown by MOCVD and later etch off the III-V substrate. These thick layers would then serve as a pseudo-substrate for MBE.

All together, it comes as no surprise that our measured external quantum efficiencies are low compared to commercial green LEDs. However, there are clear approaches available to increase each of η_i, η_r, and η_x. By addressing the improvements in just η_r and η_x only we expect the graded injector to be competitive with commercial green LEDs.

Device lifetime

Early graded injector devices grown on ZnTe exhibited evidence of potential long lifetimes. These devices operating under high injection of 100 Amps/cm^2 degraded

by 50% after ~1500 hours of continuous operation. The recent devices, grown on GaSb substrates however have much poorer operating lifetimes. Under current densities of 52 Amps/cm^2 these devices degrade, as measured by the light emission, by 50% after only ~10 hours. Figure 4.9 illustrates the lifetime characteristics for a typical graded device grown on a GaSb substrate.

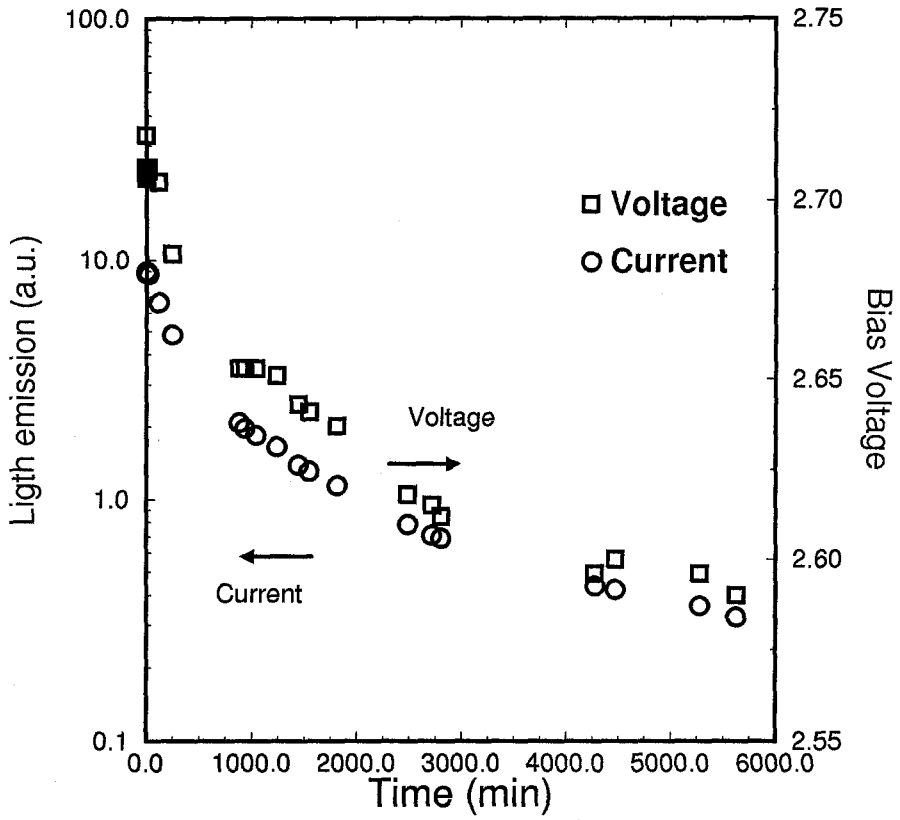

Figure 4.9: Device lifetime measurement of a graded injector LED. Device is operated under constant bias current of 52 Amps/cm^2. Light emission is measured by the photodiode current of a silicon photodetector in an integrating sphere. Bias voltage is the voltage measured across the LED.

The reason for the poor device lifetime is presently unknown. The possibilities being investigated include defect formation in the ZnTe epilayer due to nitrogen doping, or from the ZnTe growth on GaSb, either of which could degrade recombination efficiency. Another possibility is that defect formation at the graded

junction Se/Te interface leads to greater interfacial recombination and therefore reduced injection efficiency. This last reason may explain the difference in lifetimes between the early and present devices due to a difference in device operation. The earlier devices operated under high bias and may have been a high field effect device, while the present devices clearly achieve minority carrier injection as a normal p-n diode. The present devices' current voltage characteristics degrade considerably along with the optical output, which wasn't the case for the early devices. This is observed in the reduced bias voltage with time under constant bias current observed in Figure 4.9.

The present device's J-V becomes much leakier (*i.e.* greater bias current for a given bias voltage, or lower bias voltage for a given bias current) indicating greater interface space-charge recombination. Figure 4.10 plots the relation between the light emission current and bias voltage change operating under a constant bias current. This relation exhibits a thermionic behavior between the light emission and bias voltage. This suggests a dependence for the light emission (lifetime) on the injection current efficiency rather than the recombination efficiency. Therefore the lifetime degradation may be due to reduced injection efficiency rather than reduced recombination efficiency. This may result from defect formation at the graded junction Se/Te interface enhanced by the extra strain from the thick grading. The early device's lifetime may have been a measure of the active region's recombination rather than of the injection process. Therefore improvements in reducing the interfacial defects may greatly improve the device lifetime characteristics.

The precise nature of the device lifetime is still under investigation. This may turn out to be a fundamental problem associated with II-VIs. In general, the II-VI semiconductors are soft materials and may not have the robustness needed for long lifetime LEDs and laser diodes. This could prove to be an inherent physical attribute which will frustrate device development. However, strong evidence points to the lifetime problem being related to the poor Se/Te interface. This should be a tractable problem with improvements in growth technology.

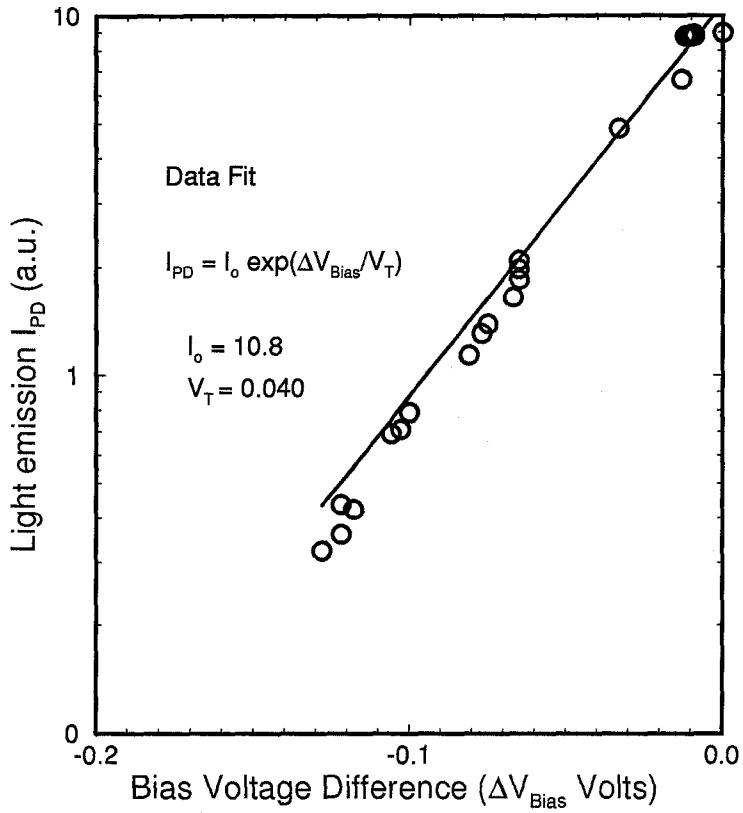

Figure 4.10: Light emission, as measured by the photodiode current of a silicon photodetector in an integrating sphere, vs. the change in bias voltage for a graded device operating under constant current. Data is taken from that of Figure 4.9. The straight line fit exhibits a thermionic related process to the lifetime degradation. This suggests a reduced injection efficienty rather than a decreased recombination efficiency in the temporal behavior of the device operation.

4.6 Conclusion and areas for future development

We have clearly demonstrated operation of the graded junction electron injector LED based on the n-CdSe/$Mg_xCd_{1-x}Se$/p-ZnTe structure. Success with the p-type doping of MBE ZnTe and the use of GaSb substrates to grow high quality ZnTe has lead to major improvements in device performance. Normal p-n diode-like LEDs with low turn-on voltages and efficient election injection into the wider band gap material have been demonstrated. Device simulations and lifetime studies suggest the graded junction Se/Te interface may play a role in the reduced and degrading injection efficiency.

A number of areas are open for additional research. Further development of the growth technology necessary to optimize the device structure should lead to increasing performance gains. Improved control of the Mg flux, via a valved Mg cell, will allow for precise thickness control of the graded $Mg_xCd_{1-x}Se$ junction and better Se/Te interface control. The incorporation of quantum structures will lead to improved recombination efficiencies. The development of substrate technology for homoepitaxial growth will be critical to improving light extraction characteristics. In addition, more sophisticated processing technology will enable greater extraction efficiencies. Most importantly, the nature of the device lifetime and failure modes should be studied.

Bibliography

[1] M.C. Phillips, M.W. Wang, J.F. Swenberg, J.O. McCaldin and T.C. McGill, *Appl. Phys. Lett.* **61**, 1962 (1992).

[2] M.C. Phillips, sl Graded Injection: A New Approach to Wide-bandgap Light Emitters, (Ph.D. thesis dissertation, CalTech, 1993).

[3] K. Itoh, *J. Phys. Soc. Japan* **22**, 1119 (1967).

[4] H. Okuyama, K. Nakano, T. Miyajima and K. Akimoto, *Jpn. J. Appl. Phys.* **30**, L1620 (1991).

[5] H. Okuyama, T. Miyajima, Y. Morinaga, F. Hiei, M. Ozawa and K. Akimoto, *Electronics Letters* **28**, 1798 (1992).

[6] A. Waag, H. Heinke, S. Scholl, C. Becker and G. Landwehr, *J. Cryst. Growth* **131**, 607 (1993).

[7] W. Strehlow and E. Cook, *J. Phys. C* **2**, 163 (1973).

[8] J.O. McCaldin, T.C. McGill and C.A. Mead, *Phys. Rev. Lett.* **36**, 56 (1976).

[9] S. Wei and A. Zunger, *Phys. Rev. Lett.* **59**, 144 (1987).

[10] M.W. Wang, J.F. Swenberg, M.C. Phillips, E.T. Yu, J.O. McCaldin, R.W. Grant and T.C. McGill, *Appl. Phys. Lett.* **64**, 3455 (1994).

[11] E. Yu, M. Phillips, J. McCaldin and T. McGill, *J. Vac. Sci. Technol. B* **9**, 2233, (1991).

[12] TEM studies were performed by Carol Garland, Department of Material Science, California Institute of Technology.

[13] P.F. Fewster, PC-HRS Version 1.0 Software, Philips Research Laboratories, Redhill, UK (Copyright 1990). The model is based on the Tagaki-Taupin [14, 15] formula adapted by P.F. Fewster *et al.* [16]

[14] S. Tagaki, *Acta. Cryst.* **15**, 1311 (1962).

[15] P. Taupin, *Bull. Soc. Fran. Miner. Cryst.* **87**, 469 (1964).

[16] P.F. Fewster, C.J. Curling, *J. Appl. Phys.* **62**, 4154, (1987).

[17] W. Shockley and W.T. Read, *Phys. Rev.* **87**, 835 (1952).

[18] M.W. Wang, M.C. Phillips, J.F. Swenberg, E.T. Yu, J.O. McCaldin and T.C. McGill, *J. Appl. Phys.* **73**, 4660 (1993).

[19] For a discussion of minority carrier injection in p-n junction diodes see Chapter 8 of S. Wang, *Fundamentals of Semiconductor Theory and Device Physics* (Prentice Hall, New Jersey, 1989).

[20] Integrating sphere model IS-040-SF from Lasphere, Inc. P.O. Box 70 Shaker Street North Sutton, NH 03260.

[21] D.L. Mathine, S.M. Durbin, R.L. Gunshor, M. Kobayashi, D.R. Menke, Z.Pei, J.Gonsalves, N. Otsuka, Q.Fu, M. Hagerott and A.V. Nurmikko, *Appl. Phys. Lett.* **55**, 268, (1989).

[22] K.H. Huang, J.G. Yu, C.P. Kuo, R.M. Fletcher, T.D. Osentowski, L.J. Stinson, M.G. Craford and A.S.H. Liao, *Appl. Phys. Lett.* **61**, 1045 (1992).

[23] F.A. Kish, F.M. Steranka, D.C. Defevere, D.A. Vanderwater, K.G. Park, C.P. Kuo, M.G. Craford and V.M. Robbins, *Appl. Phys. Lett.* **64**, 2839 (1994).

[24] Stan Gage, *Optoelectronics/Fiber-optics Application Manual*, Hewlett-Packard Company Optoelectronics Division Applications Engineering Staff, (McGraw-Hill, New York, 1981).

[25] M.W. Wang, Chapter 4, Ph.D. thesis dissertation (1994).